(1)

ARPA Semiannual Technical Report

Materials Science

December 15, 1973

Division of Engineering and Applied Physics

Harvard University

~~June 6, 1973 - May 31, 1974~~

ARPA Order Number 2440

Program Code Number 3D10

Amount of Contract $160,000.

Contract Number DAHC15-73-G16

John E. Austin
Director of Laboratories
617-495-2908

TABLE OF CONTENTS

I. FUNDAMENTALS OF LASER INDUCED ELECTRIC BREAKDOWN

Prof. N. Bloembergen

Report Summary

A review article with the title "Laser Induced Electric Breakdown in Solids" has been prepared during this period. This paper has been accepted for publication in the February 1974 issue of the IEEE Journal of Quantum Electronics. It shows the need for further experimental data on induced electric breakdown as a function of wavelength and pulse duration. Consequently a reliable, high power, mode-locked Nd-Yag laser system is being assembled to provide single diffraction limited picosecond pulses, with frequency doubling to green and ultra-violet wave lengths. Details of progress are reported below. Quantitative work on gas breakdown by 10.6 μm radiation from a CO_2 is also reported.

micrometers

Carbon Dioxide

Optical Damage in Transparent Solids

A comprehensive review paper on laser induced electric breakdown in trasnparent dielectric solids has been prepared and accepted for publication.[1] This paper was based on an invited paper delivered at an International Laser Conference in Dresden, June 1973. The material will also be the subject of an invited paper at the meeting of the Optical Society of America, to be held in Washington, D. C. in April 1974.

This review revealed a need for further quantitative data on electric breakdown in the picosecond pulse regime, and at frequencies higher than that of the ruby laser. Therefore a new Nd: Yag laser system is being constructed to provide reproducible, diffraction limited picosecond pulses. The system employs an oscillator head, pumped by a linear flashlamp and is powered by ILC digital power supplies, enabling pulsing up to 20 pps. Three similar Nd: Yag amplifier heads have been constructed. Tests are presently underway to determine the oscillator output properties. A newly designed cylindrical-ring-electrode Pockel's cell is used for single picosecond pulse extraction. It is known that placing a saturable absorber mode-locker in contact with one of the laser cavity mirror surfaces minimizes problems of satellite pulse trains and pulse noise. A contacted dye cell has been constructed and tested for this new system. Considerable experience in its use has been gained while investigating a new Kodak Q-switch dye for 1.06 microns, BIS-Ni. The laser system will be refined to a well controlled state and used for new series of picosecond pulse experiments in nonlinear spectroscopy, electron emission, and laser-induced breakdown.

Reference:

1. N. Bloembergen, IEEE Journal of Quantum Electronics, QE10, March 1974.

Investigations of Gaseous Breakdown with TEA CO_2 Lasers

Two CO_2 helical TEA lasers (3000 KW) are being used to study prebreakdown electron plasma growth in gases at high pressures and partial data has been taken in helium. Such plasma growth is a fundamental limitation on the distortionless transmission of light, and at high plasma density the medium becomes opaque, resulting in laser induced breakdown and damage.

In this experiment, the "afterglow" from the breakdown of a strong laser pulse is used as the initial electron source for a much weaker, collinear, time-delayed, second laser pulse. The breakdown threshold for the second laser pulse is measured as a function of the time interval between the pulses.

Laser induced breakdown has been extensively studied--there is the recent work in solids in this laboratory,[1] as well as the numerous studies in gases by other laboratories.[2] Briefly, previous work in this field has set the ground work for the present experiment by demonstrating that there are four stages to laser induced breakdown (pre-opaque initial electron runaway and plasma growth, past-opaque absorption, and past pulse plasma attenuation), that the mechanism for the plasma growth stage from CO_2 lasers is an electron avalanche driven by inverse bremsstrahlung, that there are several competing electron loss mechanisms, and that dirt or impurities must be avoided.

In gases, production of the initial electrons is a critical problem because there are likely to be no free electrons in the focal volume of the laser beam in a gas at room temperature. The striking laboratory demonstrations of laser induced breakdown sparks in air start from small absorbing particles in the air which provide the initial electrons thermionically.

In this experiment, the delayed pulse from the second laser hit the remains of the plasma caused by the breakdown of the first pulse, and, by varying the delay, the plasma growth during the second pulse can be studied over a wide range of initial plasma densities. Data obtained during the present reporting period are given in the graph for helium at 500 psi. There are several regions (1) for a strong second pulse and dense remanent plasma, the gas becomes opaque before the peak of the pulse is reached, (2) for the values along the heavy line through the experimental points, breakdown occurs at the peak, (3) in a small lower field and lower plasma density region bordering the experimental points, breakdown occurs after the peak (in helium at 500 psi, there are large variations in the position of the breakdown point in the tail--measurements at lower pressures have a broader breakdown region and have reproducible results in the tail , and (4) there is the low field-low plasma density region in which the gas is transparent (the gas having healed itself as far as radiation pulse at the laser frequency is concerned). Finally, there are two families of such curves--one with pressure as a parameter and one with focal volume as a parameter. But extensions of D. C. scaling laws and previous studies of loss mechanisms should reduce the number of experimental runs.

With this experiment, we hope to accurately measure the fundamental avalanche growth parameter, the rate of ionization, as a function of pressure and laser intensity after correcting for the electron loss mechanisms. This description would enable engineering predictions for the maximum operation level of a CO_2 laser amplifier or for the selective amplification of a small volume of plasma altering its properties in a controlled manner.

References:

1. E. Yablonovitch, "Optical Dielectric Strength of Alkali-Halide Crystals by Laser-Induced Breakdown," App. Phys. Lett. 19, 495 (1971).

D. W. Fradin, N. Bloembergen, P. Letellier, "Dependence of laser-induced breakdown field strength on pulse duration," Appl. Phys. Lett. 22, 635 (1973).

N. Bloembergen, "Laser Induced Electric Breakdown in Solids," IEEE J. of Quantum Electronics, QE10, March 1974.

2. E. Yablonovitch, "Similarity principles for laser-induced breakdown in gases," Appl. Phys. Lett., 23, 121 (1973).

C. De Michelis, "Laser Induced Gas Breakdown: A Bibliographical Review," IEEE J. Quantum Electron., QE-5, 188, (1969).

M. P. Hacker, D. R. Cohn, B. Lax, "Low-pressure gas breakdown with CO_2 laser radiation," Appl. Phys. Lett., 23, 392 (1973) - 50-700 torr.

R. T. Brown, D. C. Smith, "Laser-induced gas breakdown in the presence of preionization," Appl. Phys. Lett., 22, 245 (1973) - 760 torr.

M. C. Richardson, A. J. Alcock, "An Interferometric Study of CO_2 - Laser-Produced Sparks," IEEE J. Quantum Electron., QE-9, 1139 (1973) - measure high density plasma immediately after breakdown.

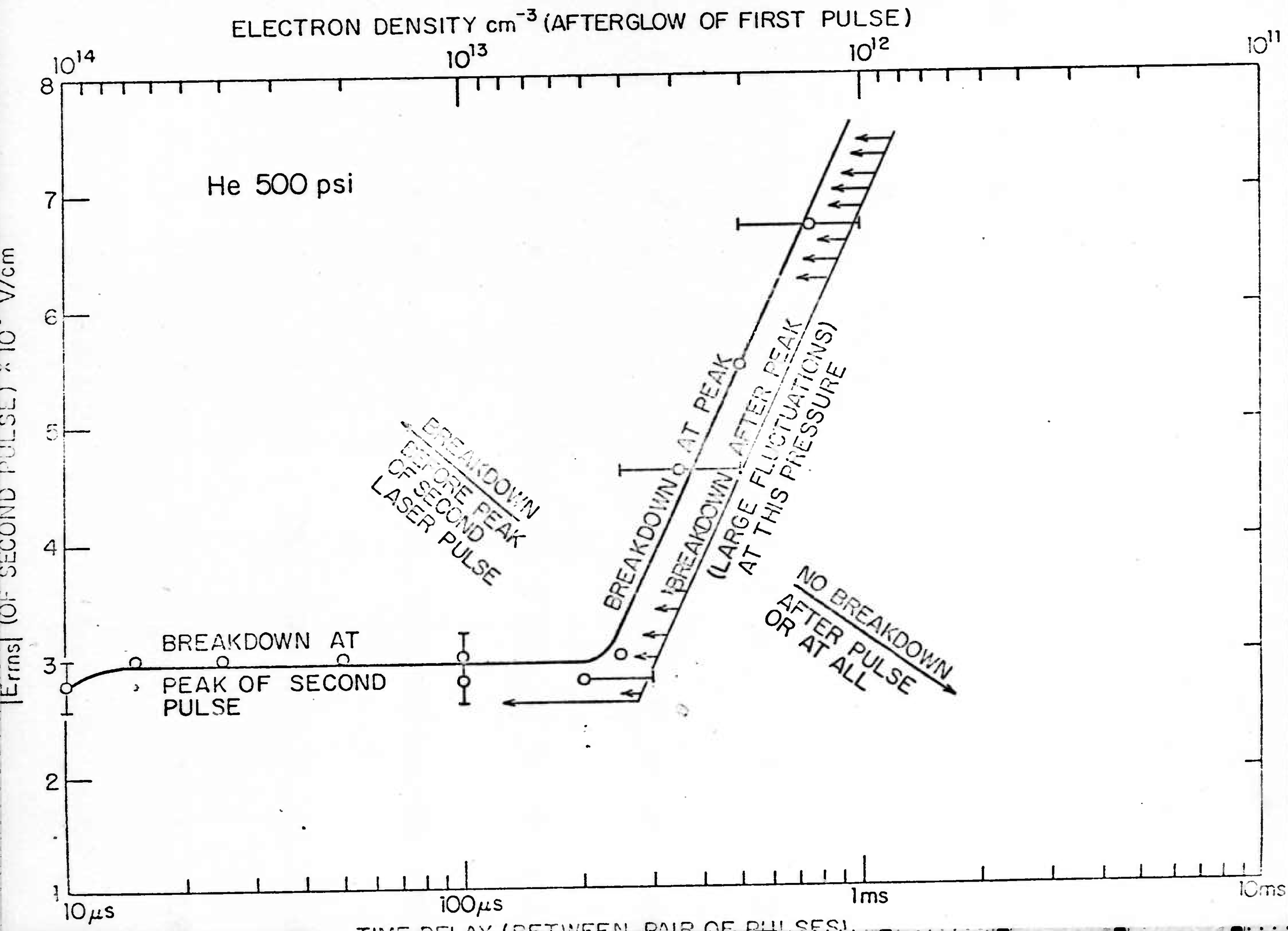

ELECTRON DENSITY cm^{-3} (AFTERGLOW OF FIRST PULSE)
10^{14}
10^{13}
10^{12}
10^{11}
He 500 psi
BREAKDOWN BEFORE PEAK OF SECOND LASER PULSE
BREAKDOWN AT PEAK
BREAKDOWN AFTER PEAK (LARGE FLUCTUATIONS) AT THIS PRESSURE
NO BREAKDOWN AFTER PULSE OR AT ALL
BREAKDOWN AT PEAK OF SECOND PULSE
10μs
100μs
1ms
10ms
1
2
3
4
5
6
7
8

II. FRACTURE MECHANICS

Profs. B. Budiansky, J. W. Hutchinson, J. L. Sanders, Jr.

Report Summary

A report was issued [Ref. 1; a copy is attached] reviewing an approach to the formulation of equations for elastic-plastic solids at finite strains which lends itself to numerical analysis. Included in the report is a generalization of J_2 flow theory (Prandtl-Reuss theory) to large strains in a form convenient for applications. Also discussed is the application of this approach to the analysis of necking-type instabilities.

Further work on the analysis of mixed mode crack problems has been completed [Ref. 2; a copy is attached]. In this work the plastic stress and strain fields at the tip of a crack are found for combined Mode I and Mode II under plane stress conditions. The solutions provide insight into the important, but poorly understood, problem of fracture under combined mode loadings.

The first report [Ref. 3; a copy is attached] in a series of studies of fully plastic crack problems has been completed. An exact solution has been obtained for a crack in a fully plastic, infinite body under anti-plane shear loading (Mode III). The solution is valid for any degree of strain hardening ranging from linear elasticity to perfect plasticity. Results are given for the dependence of the two quantities of most interest in fracture analysis, J and the crack opening displacement, on the strain hardening exponent and the applied stress. A related study for the plane strain problem has been completed and will shortly be issued as a report. Work is continuing on the application of these solutions to engineering fracture analysis where large scale plastic yielding occurs. It is this area of fracture mechanics which is currently undergoing rapid development with potential applications in many areas including reactor technology, pressure vessels and aerospace.

The work described above is jointly supported by ARPA and the Air Force Office of Scientific Research.

References:

1. FINITE STRAIN ANALYSIS OF ELASTIC-PLASTIC SOLIDS AND STRUCTURES by John W. Hutchinson, published by American Society of Mechanical Engineers in "Numerical Solution of Nonlinear Structural Problems," AMD-Vol. 6, 1973.

2. PLASTIC ANALYSIS OF MIXED MODE PLANE STRESS CRACK PROBLEMS by J. W. Hutchinson and C. F. Shih, to be published in Proceedings of the Tenth Anniversary Meeting of the Society of Engineering Science, Raleigh, North Carolina, November 1973.

3. FULL PLASTIC CRACK IN AN INFINITE BODY UNDER ANTI-PLANE SHEAR by John C. Amazigo, submitted for publication to the International Journal of Solids and Structures.

FINITE STRAIN ANALYSIS OF ELASTIC-PLASTIC SOLIDS AND STRUCTURES*

John W. Hutchinson

Division of Engineering and Applied Physics
Harvard University
Cambridge, Massachusetts

ABSTRACT

A review is given of one approach to the formulation of equations for elastic-plastic solids at finite strains which lends itself to numerical analysis. A generalization of J_2 flow theory to large strains is given which is in a form convenient for applications. Several aspects of the analysis of necking in tension are discussed from this point of view. Applications of the formulation to nonlinear plate and shell theory are also discussed.

INTRODUCTION

Most of the nonlinear theories of plates and shells are Lagrangian in character in that they employ as a reference configuration the undeformed state of the structure. In the construction of these theories it is common practice to start with a set of strain measures and strain-displacement relations (which are usually approximate in some sense), to introduce conjugate stress quantities, and to then postulate a variational principle of virtual work in terms of the variables of the theory. Equilibrium equations are obtained as the Euler equations of the variational principle. In this way the variables of the ad hoc theory are connected by exact variational equations and one or another of these principles is usually at the heart of any scheme for discretizing the equations. Budiansky (1) has emphasized the common mathematical structure shared by such ad hoc theories and a particular form of the nonlinear field equations for three-dimensional solid bodies which employs the Lagrangian strain tensor and the undeformed configuration of the body as reference. This formulation as it pertains to elastic-plastic solids will be briefly reviewed here. A finite strain version of J_2 flow theory will be discussed which fits nicely into the Lagrangian formulation. Some recent results for the problem of necking of a bar in tension will serve to illustrate the possibilities which are opened up by the application of numerical analysis methods to problems involving finite strain complications. A relatively straightforward way

---

* To appear in a proceedings, edited by R. F. Hartung, of the ASME Symposium on Numerical Solution of Nonlinear Structural Problems, to be held in November 1973 in Detroit.

to incorporate certain finite strain aspects into the elastic-plastic analysis of thin plates and shells is also discussed.

A LAGRANGIAN FORM OF THE FIELD EQUATIONS FOR ELASTIC-PLASTIC SOLIDS

Material points are identified by a set of convected coordinates x^i. Following the standard convention, superscripted indices denote contravariant components of a tensor and subscripted components the covariant components. Let g_{ij} and G_{ij} be the metric tensors of the undeformed and deformed configurations and let g^{ij} and G^{ij} be their respective inverses. Denote base vectors in the undeformed body by $\underset{\sim}{e}_i$ and their reciprocals by $\underset{\sim}{e}^i = g^{ij}\underset{\sim}{e}_j$. Similarly, the base vectors in the deformed body are denoted by $\bar{\underset{\sim}{e}}_i$ and $\bar{\underset{\sim}{e}}^i = G^{ij}\bar{\underset{\sim}{e}}_j$. Denote the displacement vector from the undeformed configuration by $\underset{\sim}{u} = u_i\underset{\sim}{e}^i = u^i\underset{\sim}{e}_i$ where $u^i = g^{ij}u_j$. The Lagrangian strain tensor is

$$\eta_{ij} = \frac{1}{2}(G_{ij} - g_{ij}) = \frac{1}{2}(u_{i,j} + u_{j,i}) + \frac{1}{2}\, u^k{}_{,i}u_{k,j} \,, \tag{1}$$

where the comma denotes covariant differentiation with respect to the undeformed metric.

The exact statement of the principle of virtual work based on the undeformed configuration is (1, 2, 3)

$$\int_V \tau^{ij}\delta\eta_{ij}\,dV = \int_S T^i\delta u_i\,dS \,, \tag{2}$$

where

$$\delta\eta_{ij} = \frac{1}{2}(\delta u_{i,j} + \delta u_{j,i}) + \frac{1}{2}(u^k{}_{,i}\delta u_{k,j} + u^k{}_{,j}\delta u_{k,i}) \,. \tag{3}$$

Here, dV and dS are the volume and surface elements of the undeformed body, τ^{ij} are the contravariant components of the symmetric Kirchhoff stress defined with respect to the deformed base vectors, and $\underset{\sim}{T} = T^i\underset{\sim}{e}_i$ is the surface traction vector per unit undeformed area. With $\underset{\sim}{n} = n_i\underset{\sim}{e}^i$ denoting the unit normal to a surface element in the undeformed body, the surface traction $\underset{\sim}{T}$ acting on this surface element in the deformed body is

$$\underset{\sim}{T} = (\tau^{ij} + \tau^{mj}u^i{}_{,m})n_j\underset{\sim}{e}_i \,. \tag{4}$$

Let $g = |g_{ij}|$ and $G = |G_{ij}|$. The contravariant components of the Cauchy stress are given by

$$\sigma^{ij} = (g/G)^{1/2}\tau^{ij} \,. \tag{5}$$

The surface traction vector per unit current area $\bar{\underset{\sim}{T}}$ acting on a surface whose current unit normal is $\bar{\underset{\sim}{n}} = \bar{n}_i\bar{\underset{\sim}{e}}^i$ is given by

$$\bar{\underset{\sim}{T}} = \sigma^{ij}\bar{n}_i\bar{\underset{\sim}{e}}_j \,. \tag{6}$$

The incremental form of the principle of virtual work is

$$\int_V \{\dot{\tau}^{ij}\delta\eta_{ij} + \tau^{ij}\dot{u}^k{}_{,j}\delta u_{k,i}\}dV = \int_S \dot{T}^i\delta u_i dS \; , \qquad (7)$$

and the associated equilibrium equations are

$$\dot{\tau}^{ij}{}_{,j} + (\dot{\tau}^{kj}u^i{}_{,k})_{,j} + (\tau^{kj}\dot{u}^i{}_{,k})_{,j} = 0 \; . \qquad (8)$$

Hill (4) has discussed the general framework for the classical rate-constitutive relations for elastic-plastic solids with smooth yield surfaces at finite strain. Using the convected rate of the contravariant components of the Kirchhoff stress, the rate-constitutive relation can be expressed in the general form

$$\dot{\tau}^{ij} = L^{ijk\ell}\dot{\eta}_{k\ell} \qquad (9a)$$

where

$$L^{ijk\ell} = \mathscr{L}^{ijk\ell} - \frac{\alpha}{q} m^{ij}m^{k\ell} \; . \qquad (9b)$$

For stresses within the yield surface $\alpha = 0$ and for stresses on the yield surface

$$\alpha = 1 \quad \text{if} \quad m^{ij}\dot{\eta}_{ij} \geq 0 \quad \text{and} \quad \alpha = 0 \quad \text{if} \quad m^{ij}\dot{\eta}_{ij} < 0 \; . \qquad (10)$$

Here, $\underset{\sim}{\mathscr{L}}$ is the current tensor of elastic moduli for this choice of stress-rate and it is assumed that $\mathscr{L}^{ijk\ell} = \mathscr{L}^{k\ell ij}$. The tensor of instantaneous moduli for loading is $\underset{\sim}{L}$ and $\underset{\sim}{m}$ is the current unit tensor normal to the yield surface in strain-rate space. The current level of strain hardening is determined by q and the strain-rate is given by

$$\dot{\eta}_{ij} = \frac{1}{2}(\dot{u}_{i,j} + \dot{u}_{j,i}) + \frac{1}{2}(u^k{}_{,j}\dot{u}_{k,i} + u^k{}_{,i}\dot{u}_{k,j}) \; . \qquad (11)$$

Introduce the functional of $\dot{\underset{\sim}{u}}$,

$$I = \frac{1}{2}\int_V \{\dot{\tau}^{ij}\dot{\eta}_{ij} + \tau^{ij}\dot{u}^k{}_{,i}\dot{u}_{k,j}\}dV - \int_{S_T} \dot{T}^i\dot{u}_i dS \; , \qquad (12)$$

where $\dot{\underset{\sim}{T}}$ is prescribed on S_T and $\dot{\underset{\sim}{u}}$ on S_u and where the stress-rates $\dot{\tau}^{ij}$ are regarded to be a function of the strain-rates through (9) and (10). The variational principle governing the incremental boundary value problem is (5)

$$\delta I = 0 \qquad (13)$$

for all admissible δu_i which vanish on S_u. Equations (12) and (13) reduce to the well-known principle for the classical small strain and small rotation theory.

The above variational equation provides the theoretical foundation for a variety of possible numerical solution methods. Chen (6) used a

Kantorovich approximation method in conjunction with this variational equation to analyze necking in a bar. Needleman (7) used the principle as the basis for a finite element method solution to a large strain problem related to void growth and coalescence in metals. The same method was applied to the tensile necking problem (8) and some results from this calculation will be discussed in a later section.

Oden (9) has given an extensive review of the work on the development of finite element methods for the large strain analysis of elastic solids. Hibbitt, Marcal and Rice (10) have discussed the formation of finite element equations based on a Lagrangian formulation for elastic-plastic solids which is essentially identical to that reviewed above. The choice of a Lagrangian based numerical scheme as opposed to a Eulerian scheme, for example, is dictated by a number of considerations. Since the variational functional (12) is based on the undeformed configuration, the finite element (or finite difference) grid remains fixed. For this reason, the Lagrangian approach can be attractive if the undeformed configuration is a simple one. In the simplest finite element scheme, used by Needleman, the displacement fields within triangular elements are taken to be linear functions of the reference coordinates and thus the strains, stresses and moduli are constant within each element. At each stage of the calculation procedure the moduli must be updated in a straightforward way which can be illustrated by one possible prescription for the moduli in the next section. As in any elastic-plastic calculation, the loading-unloading behavior associated with an incremental step must in general be handled in an iterative fashion.

A FINITE STRAIN GENERALIZATION OF J_2 FLOW THEORY

Small strain formulations of strain-hardening plasticity involve the stress deviator s_{ij} and the J_2 invariant where in Cartesian coordinates

$$s_{ij} = \tau_{ij} - \frac{1}{3}\tau_{pp}\delta_{ij} \quad \text{and} \quad J_2 = \frac{1}{2}s_{ij}s_{ij} , \tag{14}$$

where δ_{ij} is the Kronecker delta. It is usually unnecessary to give a precise definition to the stress measure in small strain formulations and for the moment the precise meaning of τ_{ij} will be left ambiguous. In one of the most widely used plasticity theories, J_2 flow theory, the strain-rate is given in terms of the stress-rate by

$$\dot{\eta}_{ij} = \frac{1}{E}[(1+\nu)\delta_{ik}\delta_{j\ell} - \nu\delta_{ij}\delta_{k\ell}]\dot{\tau}_{k\ell} + \frac{\alpha f}{E}s_{ij}\dot{J}_2 , \tag{15}$$

where

$$\left.\begin{aligned} &\alpha = 1 \quad \text{if} \quad \dot{J}_2 = s_{ij}\dot{\tau}_{ij} \geq 0 \quad \text{and} \quad J_2 = (J_2)_{max} \\ &\alpha = 0 \quad \text{if} \quad \dot{J}_2 < 0 \quad \text{or} \quad J_2 < (J_2)_{max} \end{aligned}\right\} \tag{16}$$

In (15) E is Young's modulus, ν is Poisson's ratio and f is a function of J_2 which can be chosen to make (15) coincide with any monotonic proportional loading history.

The inversion of (15) is

$$\dot{\tau}_{ij} = \frac{E}{1+\nu}[\delta_{ik}\delta_{j\ell} + \frac{\nu}{1-2\nu}\delta_{ij}\delta_{k\ell}]\dot{\eta}_{k\ell} - \frac{E}{1+\nu}\frac{\alpha}{q}s_{ij}s_{k\ell}\dot{\eta}_{k\ell} , \tag{17}$$

where if $J_2 = (J_2)_{max}$ $\alpha = 1$ if $s_{ij}\dot{\eta}_{ij} \geq 0$ and $\alpha = 0$ if $s_{ij}\dot{\eta}_{ij} < 0$.
Also, f and q are connected by

$$q = f/[(1+\nu) + 2fJ_2] \ . \tag{18}$$

The expression for the moduli in the small strain formulation is thus

$$L_{k\ell ij} = L_{ijk\ell} = \frac{E}{1+\nu}\left[\frac{1}{2}(\delta_{ik}\delta_{j\ell} + \delta_{i\ell}\delta_{jk}) + \frac{\nu}{1-2\nu}\delta_{ij}\delta_{k\ell} - \frac{\alpha}{q}s_{ij}s_{k\ell}\right] \ . \tag{19}$$

If a uniaxial tension curve is used to determine f and q, one finds that they are given by

$$[1 + \frac{4}{3}J_2 f]^{-1} = (q - 2J_2)/[q - \frac{2}{3}(1-2\nu)J_2] = \frac{E_t}{E} \ , \tag{20}$$

where E_t is the tangent modulus which is regarded as a function of J_2 through the connection with the tensile stress, $J_2 = \sigma^2/3$.

There are many possible ways to generalize the above relation to a finite strain formulation (11, 12, 13). The one selected for discussion is a special case of Hill's (4) general class (9) and (10) and has a form particularly suitable to a Lagrangian approach. It is a slightly modified version of a relation proposed by Budiansky (14). As in the small strain version the theory employs a J_2 invariant of the stress to describe the yield surface and thus does not account for any Bauschinger effect. It is also assumed that the strains are not so large that appreciable elastic anisotropy develops.

The contravariant components of the Kirchhoff stress τ^{ij} will be used in the formulation and a deviator stress tensor is defined according to

$$s^{ij} = \tau^{ij} - \frac{1}{3}G^{ij}G_{k\ell}\tau^{k\ell} \tag{21}$$

where $\underset{\sim}{G}$ is the metric tensor in the deformed system as previously introduced so that with this definition $G_{ij}s^{ij} = 0$. We take J_2 to be defined in terms of the stress deviator by

$$J_2 = \frac{1}{2}G_{ik}G_{j\ell}s^{ij}s^{k\ell} \ . \tag{22}$$

If the coordinate system in the deformed body happens to be Cartesian then (21) and (22) have the same form as (14). Since the undeformed configuration is used as reference the deformed configuration will not, in general, be Cartesian and the general tensor formulation of (21) and (22) is necessary.

If the Cauchy stress (5) is used in forming J_2 in place of the Kirchhoff stress, the invariant will differ from (22) by a multiplicative factor $G/g = (d\bar{V}/dV)^2$, where $d\bar{V}/dV$ is the deformed volume per unit undeformed volume. The volume change in the relation given below arises entirely from the elastic part of the strain-rate. As long as the hydrostatic pressure is very small compared to the elastic bulk modulus, there is little experimental evidence to point to one choice over the other in the formulation of a yield criterion as discussed by Lee (12).

With J_2 defined by (22) it can be shown that the rate of change of

J_2 is

$$\dot{J}_2 = G_{ik}G_{j\ell}s^{k\ell}\overset{*}{\tau}^{ij} . \tag{23}$$

Here the $\overset{*}{\tau}^{ij}$ are the contravariant components of the symmetric Jaumann rate of change of the Kirchhoff stress which are related to the convected rate $\dot{\tau}^{ij}$ by

$$\overset{*}{\tau}^{ij} = \dot{\tau}^{ij} + G^{ik}\tau^{j\ell}\dot{\eta}_{k\ell} + G^{jk}\tau^{i\ell}\dot{\eta}_{k\ell} . \tag{24}$$

The generalization of (15) we will use is

$$\dot{\eta}_{ij} = \frac{1}{E}[(1+\nu)G_{ik}G_{j\ell} - \nu G_{ij}G_{k\ell}]\overset{*}{\tau}^{k\ell} + \frac{\alpha f}{E}G_{ik}G_{j\ell}s^{k\ell}\dot{J}_2 \tag{25}$$

with

$$\left.\begin{aligned} \alpha = 1 \quad \text{if} \quad \dot{J}_2 \geq 0 \quad \text{and} \quad J_2 = (J_2)_{max} \\ \alpha = 0 \quad \text{if} \quad \dot{J}_2 \leq 0 \quad \text{or} \quad J_2 < (J_2)_{max} \end{aligned}\right\} \tag{26}$$

In (25) f is regarded as a function of J_2, and E and ν are taken to be fixed constants corresponding to their values in the undeformed state. The second part of (25) is regarded as the plastic strain-rate; and since $G_{ij}s^{ij} = 0$, the plastic volume change is zero.

In the absence of plastic deformation (25) is a hypo-elastic relation in that the relation cannot be integrated to give the strains in terms of the stresses. Curiously, though, it is possible to write the work done by the stresses per unit original volume in terms of the stresses (and the deformed metric tensor) as

$$\int_0 \tau^{ij} d\eta_{ij} = \frac{1}{2E}[(1+\nu)J_2 + \frac{1}{3}(1-2\nu)(G_{ij}\tau^{ij})^2] . \tag{27}$$

The inversion of (25) is

$$\overset{*}{\tau}^{ij} = \frac{E}{1+\nu}[G^{ik}G^{j\ell} + \frac{\nu}{1-2\nu}G^{ij}G^{k\ell}]\dot{\eta}_{k\ell} - \frac{E}{1+\nu}\frac{\alpha}{q}s^{ij}s^{k\ell}\dot{\eta}_{k\ell} . \tag{28}$$

with

$$\left.\begin{aligned} \alpha = 1 \quad \text{if} \quad s^{k\ell}\dot{\eta}_{k\ell} \geq 0 \quad \text{and} \quad J_2 = (J_2)_{max} \\ \alpha = 0 \quad \text{if} \quad s^{k\ell}\dot{\eta}_{k\ell} < 0 \quad \text{or} \quad J_2 < (J_2)_{max} \end{aligned}\right\} \tag{29}$$

The same relation (18) holds between f and q as in the small strain formulation. Using (24) the rate-constitutive relation can be cast into the form (9) involving $\dot{\tau}^{ij}$ and appropriate to the present formulation, i.e.,

$$\dot{\tau}^{ij} = L^{ijk\ell}\dot{\eta}_{k\ell} . \tag{30}$$

The instantaneous moduli are

$$L^{ijk\ell} = L^{k\ell ij} = \frac{E}{1+\nu}\left[\frac{1}{2}(G^{ik}G^{j\ell}+G^{i\ell}G^{jk})+\frac{\nu}{1-2\nu}G^{ij}G^{k\ell}-\frac{\alpha}{q}s^{ij}s^{k\ell}\right]$$

$$-\frac{1}{2}\left[G^{ik}\tau^{j\ell}+G^{jk}\tau^{i\ell}+G^{i\ell}\tau^{jk}+G^{j\ell}\tau^{ik}\right] \qquad (31)$$

with α obeying (29).

If data from a uniaxial stress-strain curve is used to determine f and q one finds by specializing (25) to pure tension that, instead of (20),

$$[1+\frac{4}{3}J_2f]^{-1} = (q-2J_2)/[q-\frac{2}{3}(1-2\nu)J_2] = \left(\frac{G}{g}\right)^{1/2}\left[\frac{E_t}{E}+\frac{\sigma}{E}(1-2\bar{\nu})\right] \quad . \qquad (32)$$

The tensile data in this equation is considered to be known as a function of the true stress σ . In simple tension $J_2 = (G/g)\sigma^2/3$. The tangent modulus E_t is now defined as $E_t = d\sigma/d\varepsilon$, where ε is the logarithmic, or natural, tensile strain. The instantaneous contraction ratio is defined to be $\bar{\nu} = -d\varepsilon_2/d\varepsilon$, where ε_2 is the logarithmic strain transverse to the tensile direction. For an elastically incompressible material, $\nu = \bar{\nu} = 1/2$ and $G/g = 1$ so that (32) reduces to the small strain expression (20) with the proper interpretation of E_t .

As has been discussed by many authors, two conditions are required for the small strain relation to provide an accurate approximation to a full finite strain version. For the purpose of discussion choose a Cartesian system in the undeformed body. If the strains are sufficiently small the distinction between the deformed and undeformed metric tensors in (31) can be ignored. Secondly, if the stresses are small compared to the instantaneous moduli then the second set of bracketed terms in (31) can be neglected compared to the first. In addition, (32) becomes (20), and the rate-constitutive relation becomes indistinguishable from the small strain version.

The above relation is due essentially to Budiansky (14). His original suggestion is identical in all respects except that the contravariant components of the Cauchy stress (5) σ^{ij} are used everywhere in place of the contravariant components of Kirchhoff stress τ^{ij} in equations (21) through (31). In particular, the deviator components (21) are formed from the Cauchy stress components and J_2 is based on these deviator components. Similarly, $\overset{*}{\tau}{}^{ij}$ and $\dot{\tau}^{ij}$ are replaced in (24) by $\overset{*}{\sigma}{}^{ij}$ and $\dot{\sigma}^{ij}$, which are the Jaumann and convected rates, respectively, of the contravariant components of the Cauchy stress. In this alternative formulation equations (21) through (31) remain unchanged although (27) is now interpreted as the stress work per unit deformed volume.

One feature which is particularly attractive about this second form is that, instead of (32), f and q are given by the formulas for the classical small strain version (20) where E_t is the tangent modulus of the true stress-natural strain curve in uniaxial tension. The one drawback of the version formulated in the form of the Cauchy stress is that when the moduli are converted to the form (9) involving $\dot{\tau}^{ij}$, the moduli do not satisfy the symmetry $L^{ijk\ell} = L^{k\ell ij}$ required for the variational principle (13) to hold. This can be noted directly using the relation

$$\dot{\tau}^{ij} = (G/g)^{1/2}\dot{\sigma}^{ij} + \tau^{ij}G^{k\ell}\dot{\eta}_{k\ell} \, . \tag{33}$$

For elastically incompressible solids the two versions are obviously identical. Numerically the difference between the two formulations will be inconsequential as long as the pressure is small compared to the bulk modulus.

APPLICATIONS TO NECKING ANALYSIS

In the analysis of necking in tension it is essential to use a bona fide finite strain formulation. The above formulation of the field equations has been used in the analysis of two separate aspects of necking of a solid circular cylindrical bar in tension (6, 8, 15).

First consider a bar whose ends are subject to a prescribed uniform relative axial displacement in such a way that the ends remain free of tangential traction and the lateral surface is traction-free. For these ideal boundary conditions, the uniform state of uniaxial tension is an exact solution at all values of the relative end displacement. Necking will start as a bifurcation from the uniform state. Bifurcation first becomes possible at the value of the elongation where there first exists a nonzero displacement-rate field $\dot{u}_i$ such that

$$\int_V \{L^{ijk\ell}\dot{\eta}_{ij}\dot{\eta}_{k\ell} + \tau^{ij}\dot{u}^k{}_{,i}\dot{u}_{k,j}\}dV = 0 \, , \tag{34}$$

where the moduli $\underset{\sim}{L}$ are given by (31) with $\alpha = 1$. Here the strain-rate is given by (11) and the axial component of the eigenmodal displacement-rate must vanish on the ends of the specimen.

Denote the true stress and natural strain associated with the state at which the maximum total load of the cylindrical bar is attained by σ_m and ε_m, respectively. Miles (16) has proved that bifurcation cannot occur before the maximum load is attained. The axisymmetric bifurcation problem for an incompressible bar has been studied within the context of the full three-dimensional formulation in (15, 16, 17). Let R_m and L_m denote the radius and length of the specimen when the maximum load is attained and let $\gamma = \pi R_m/L_m$. For an incompressible material characterized by (31), the true stress and natural strain at bifurcation, σ_c and ε_c respectively, are given by the expressions (15)

$$\sigma_c = \sigma_m + \left\{1 - \left.\frac{dE_t}{d\sigma}\right|_m\right\}^{-1}\left\{\frac{\gamma^2}{8}\sigma_m + \frac{\gamma^4}{192}\mu\right\} + \ldots \tag{35a}$$

and

$$\varepsilon_c = \varepsilon_m + \left\{1 - \left.\frac{dE_t}{d\sigma}\right|_m\right\}^{-1}\left\{\frac{\gamma^2}{8}\sigma_m + \frac{\gamma^4}{192}\mu\right\} + \ldots \, , \tag{35b}$$

which are asymptotically exact for small γ. In these formulas $\mu = E/3$ is the elastic shear modulus of the incompressible material, and $(dE_t/d\sigma)_m$ denotes the derivative of the tangent modulus of the true stress-natural strain curve with respect to the true stress and evaluated at the maximum load.

An example presented in (15) uses the Ramberg-Osgood tensile relation

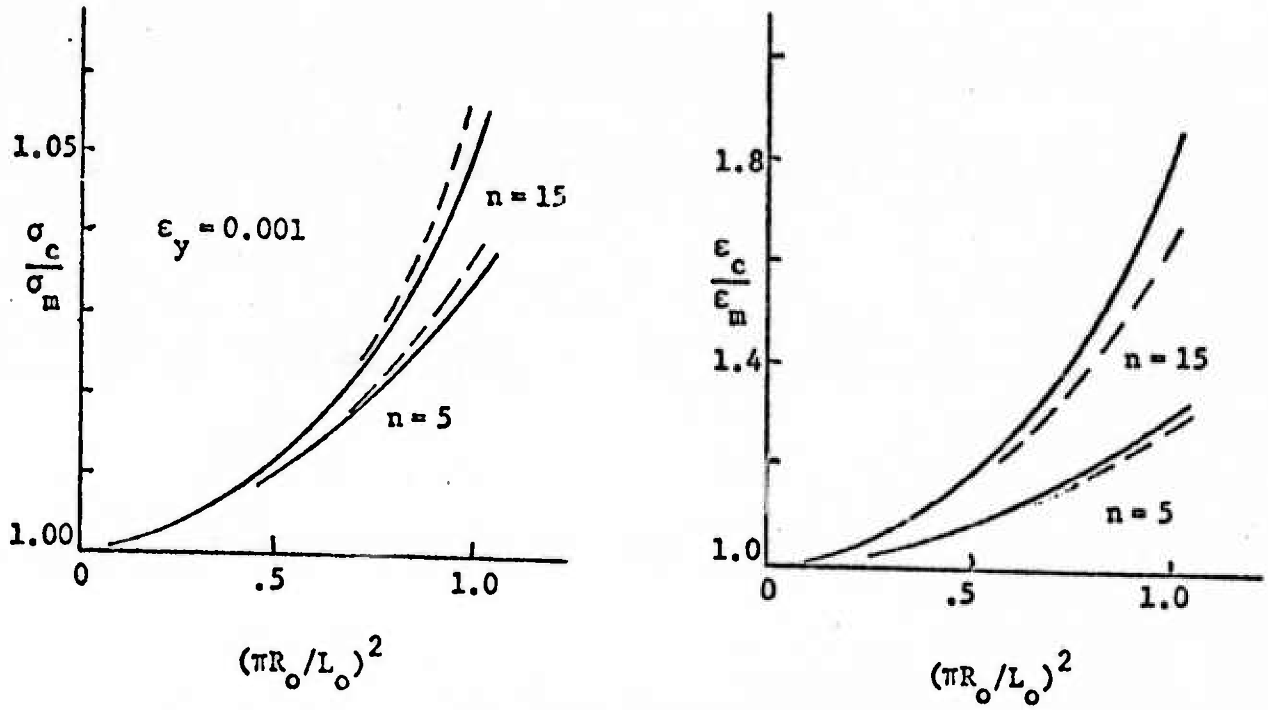

Fig. 1 Tensile bifurcation of a solid cylindrical specimen of an incompressible material with a Ramberg-Osgood tensile stress-strain relation. See (15) for an accurate plot. (Asymptotic results ----------; Exact results ——————)

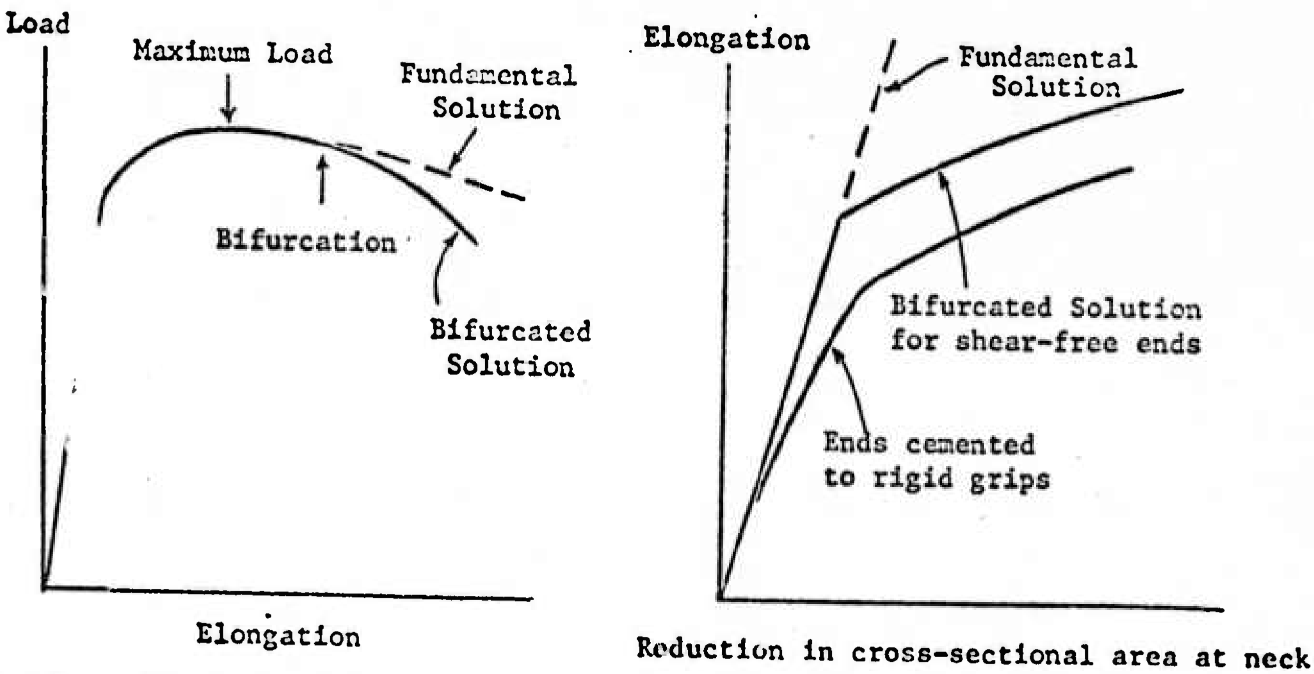

Fig. 2 Schematic of results of a numerical analysis of necking of a solid cylindrical bar from (8).

between the true stress and natural strain, i.e.,

$$\frac{\varepsilon}{\varepsilon_y} = \frac{\sigma}{\sigma_y} + \frac{3}{7}\left(\frac{\sigma}{\sigma_y}\right)^n , \tag{36}$$

where ε_y and $\sigma_y \equiv E\varepsilon_y$ are the effective yield strain and yield stress and n is the hardening exponent. For this case Eqs. (35) become

$$\frac{\sigma_c}{\sigma_m} \cong 1 + \frac{1}{n}\left(\frac{\gamma^2}{8} + \frac{\gamma^4}{192}\frac{\mu}{\sigma_m}\right) \tag{37a}$$

and

$$\frac{\varepsilon_c}{\varepsilon_m} \cong 1 + \frac{1}{n\varepsilon_m}\left(\frac{\gamma^2}{8} + \frac{\gamma^4}{192}\frac{\mu}{\sigma_m}\right) . \tag{37b}$$

Figure 1 displays plots of σ_c/σ_m and $\varepsilon_c/\varepsilon_m$ as a function of $\pi R_o/L_o$ where where R_o and L_o are the undeformed radius and length of the bar. The dashed line curves are derived from the asymptotic formulas (37) and the solid line curves are the exact results for arbitrarily large $\pi R_o/L_o$ (which require some numerical analysis in their evaluation).

Needleman (8) used the variational principle of the previous section to formulate a finite element scheme and applied it to the necking problem. He considered elastically compressible solids and used the moduli (31) together with an inconsequential approximation in which the right-hand-side of (32) is replaced by E_t/E . The axisymmetric eigenvalue problem governing bifurcation was solved using a finite element method and the post-bifurcation calculation was carried until a point where the specimen had undergone significant necking down. Figure 2 depicts the character of his solution in a typical specimen with $R_o/L_o = 4$. Bifurcation occurs beyond the maximum load and from that point on the solution for the necking specimen turns down from the fundamental solution for the uniform specimen which undergoes no bifurcation. The second part of the plot shows that bifurcation marks the onset of the rapid contraction at the neck.

Included in the second plot are results for a calculation (8) for another set of boundary conditions where the ends of the bar are considered to be cemented to rigid grips. In this case no bifurcation occurs. Instead departure from the uniform state occurs with the first application of load. The maximum load was found to be essentially the same as in the other case; but as can be seen from the plot, significant necking starts at somewhat lower elongations.

As mentioned previously, Chen (6) used the same formulation together with a Kantorovich approximation method to study the same problem. He considered the shear-free end conditions case and initiated necking by introducing a small initial axisymmetric imperfection. This same technique was used by Ocias (16) in his study of tensile necking under plane stress and plane strain conditions. However, Ocias's approach was based on a Eulerian formulation and his numerical scheme derived from a discretization of the governing differential equations directly.

APPLICATIONS TO THIN PLATE AND SHELL PROBLEMS

As emphasized in the Introduction, the structure of the field equations as developed for the three-dimensional solid closely resembles the structure of the equations for the most widely used nonlinear theories of plates and shells. In most applications involving structural materials, whether the response is elastic or elastic-plastic, the strains are small and the significant geometric nonlinearity is due to rotations. In a first order theory in which the strains are assumed to vary linearly through the thickness the inplane Lagrangian strain tensor is often approximated by

$$\eta_{\alpha\beta} = E_{\alpha\beta} + zK_{\alpha\beta} \qquad (\alpha = 1,2\ ;\ \beta = 1,2)\ , \tag{38}$$

where $E_{\alpha\beta}$ and $K_{\alpha\beta}$ are the stretching and bending strain tensors of the middle surface. The coordinate z is measured along the normal to middle surface in the undeformed shell. The stretching and bending strains are expressed in terms of the displacements of the middle surface in directions normal and tangential to the undeformed middle surface.

The internal virtual work is approximated by

$$\int_V \tau^{\alpha\beta}\delta\eta_{\alpha\beta}dV = \int_A \{M^{\alpha\beta}\delta K_{\alpha\beta} + N^{\alpha\beta}\delta E_{\alpha\beta}\}dA\ , \tag{39}$$

where dA is the element of the undeformed middle surface. The bending moment and resultant stress tensors are related to the Kirchhoff stress tensor by

$$N^{\alpha\beta} = \int_{-t/2}^{t/2} \tau^{\alpha\beta}dz \quad \text{and} \quad M^{\alpha\beta} = \int_{-t/2}^{t/2} \tau^{\alpha\beta}zdz\ , \tag{40}$$

where t is the thickness of the undeformed shell. The contravariant components of the Kirchhoff stress enter into these expressions because the Lagrangian strain tensor has been used along with the choice of the undeformed body as the reference configuration.

Suppose the three-dimensional rate-constitutive relation is of the form discussed in the previous sections for the finite strain formulation, i.e.,

$$\dot{\tau}^{ij} = L^{ijk\ell}\dot{\eta}_{k\ell}\ . \tag{41}$$

The assumption of approximate plane stress in a first order plate or shell theory requires $\eta_{\alpha 3} = 0$ for $\alpha = 1,2$ and $\tau^{33}\delta\eta_{33} = 0$, i.e., $\tau^{33} = 0$. Thus from (41)

$$\dot{\eta}_{33} = -(L^{\alpha\beta 33}/L^{3333})\dot{\eta}_{\alpha\beta}\ . \tag{42}$$

The plane stress moduli $\bar{\underset{\sim}{L}}$ relating the inplane stress-rates and strain-rates, i.e.,

$$\dot{\tau}^{\alpha\beta} = \bar{L}^{\alpha\beta\kappa\gamma}\dot{\eta}_{\kappa\gamma}\ , \tag{43}$$

are given by

$$\bar{L}^{\alpha\beta\kappa\gamma} = L^{\alpha\beta\kappa\gamma} - L^{\alpha\beta 33}L^{33\kappa\gamma}/L^{3333}\ . \tag{44}$$

From (40) the rate-constitutive relations written in terms of the stress-rate and strain-rate quantities of the plate or shell theory are

$$\overset{\bullet}{N}^{\alpha\beta} = H_{(1)}^{\alpha\beta\kappa\gamma}\overset{\bullet}{E}_{\kappa\gamma} + H_{(2)}^{\alpha\beta\kappa\gamma}\overset{\bullet}{K}_{\kappa\gamma} \tag{45}$$

$$\overset{\bullet}{M}^{\alpha\beta} = H_{(2)}^{\alpha\beta\kappa\gamma}\overset{\bullet}{E}_{\kappa\gamma} + H_{(3)}^{\alpha\beta\kappa\gamma}\overset{\bullet}{K}_{\kappa\gamma} \tag{46}$$

where

$$H_{(i)}^{\alpha\beta\kappa\gamma} = \int_{-t/2}^{t/2} \bar{L}^{\alpha\beta\kappa\gamma} z^{i-1} dz \ . \tag{47}$$

In particular, note that for the case of a flat plate with $K_{\alpha\beta} = 0$ and $E_{\alpha\beta}$ uniform through the thickness, Eq. (45) gives exactly the same relation between $\overset{\bullet}{N}^{\alpha\beta}$ and $\overset{\bullet}{E}_{\alpha\beta}$ as would be obtained from the full finite strain formulation by integrating through the thickness.

Equations (38) through (47) constitute a full complement of equations for first order plate and shell theories including finite strain effects. If the moduli $\underset{\sim}{L}$ given by (31) or some similar prescription are used, then the quantities needed for updating $\underset{\sim}{L}$ from one incremental step to another are contained in the above set of equations.

If the strains are small _and_ the stress levels are low compared to the instantaneous moduli, then as discussed previously the finite strain formulation can be replaced by a small strain formulation in which it is not necessary to give a precise definition to the stress measure. Most plastic buckling problems in thin plates and shells fall into this category. Typically, the stresses at buckling are proportional to the product of an instantaneous modulus and some ratio of the thickness to a characteristic length much greater than the thickness. On the other hand, in problems involving the onset of necking or bulging, for example, it may be essential to use an appropriate finite strain formulation even when the strains are small. As long as the characteristic length of the deformation field is large compared to the thickness one can expect the first order theory to have approximate validity. Of course, once the characteristic deformation length becomes on the order of the thickness, as in the advanced stages of necking, the first order theory is no longer applicable.

ACKNOWLEDGMENTS

This work was supported in part by the Air Force Office of Scientific Research under Grant AFOSR-73-2476, in part by the Advanced Research Projects Agency under Contract DAHC 15-73-C-16, and by the Division of Engineering and Applied Physics, Harvard University.

REFERENCES

1. Budiansky, B., "Remarks on Theories of Solid and Structural Mechanics", _Problems of Hydrodynamics and Continuum Mechanics_, SIAM, Philadelphia, 1969, pp. 77-83.

2. Bolotin, V. V., _Nonconservative Problems of the Theory of Elastic Stability_, English translation edited by Herrmann, G., Macmillan, New York, 1963.

3. Green, A. E. and Zerna, W., Theoretical Elasticity, 2nd Ed., Oxford University Press, Oxford, 1968.

4. Hill, R., "On the Classical Constitutive Relations for Elastic-Plastic Solids", Recent Progress in Applied Mechanics, the Folke Odqvist Volume, Almqvist and Wiksell, Stockholm, 1967, pp. 241-249.

5. Hill, R., "Bifurcation and Uniqueness in Nonlinear Mechanics of Continua", the Muskhelishvili Volume, SIAM, Philadelphia, 1961, pp. 155-164.

6. Chen, W. H., "Necking of a Bar", International Journal of Solids and Structures, Vol. 7, 1971, pp. 685-717.

7. Needleman, A., "Void Growth in an Elastic-Plastic Medium", Journal of Applied Mechanics, Vol. 39, 1972, pp. 964-970.

8. Needleman, A., "A Numerical Study of Necking in Circular Cylindrical Bars", Journal of the Mechanics and Physics of Solids, Vol. 20, 1972, pp. 111-127.

9. Oden, J. T., Finite Elements of Nonlinear Continua, McGraw-Hill, New York, 1972.

10. Hibbitt, H. D., Marcal, P. V. and Rice, J. R., "A Finite Element Formulation for Problems of Large Strain and Large Displacement", International Journal of Solids and Structures, Vol. 6, 1970, pp. 1069-1086.

11. Green, A. E. and Naghdi, P. M., "A General Theory of an Elastic-Plastic Continuum", Archive for Rational Mechanics and Analysis, Vol. 18, 1965, pp. 251-281.

12. Lee, E. H., "Elastic-Plastic Deformation at Finite Strains", Journal of Applied Mechanics, Vol. 36, 1969, pp. 1-6.

13. Willis, J. R., "Some Constitutive Equations Applicable to Problems of Large Dynamic Plastic Deformations", Journal of the Mechanics and Physics of Solids, Vol. 17, 1969, pp. 359.

14. Budiansky, B., (unpublished work) see References 6, 7, or 8.

15. Hutchinson, J. W. and Miles, J. P., "Bifurcation Analysis of the Onset of Necking in an Elastic-Plastic Cylinder under Uniaxial Tension", to be published in Journal of the Mechanics and Physics of Solids, Vol. 21, 1973.

16. Miles, J. P., "Bifurcation in Plastic Flow under Uniaxial Tension", Journal of the Mechanics and Physics of Solids, Vol. 19, 1971, pp. 89-102.

17. Cheng, S. Y., Ariaratnam, S. T. and Dubey, R. N., "Axisymmetric Bifurcation in an Elastic-Plastic Cylinder under Axial Load and Lateral Hydrostatic Pressure", Quarterly of Applied Mathematics, Vol. 29, 1971, pp. 41-51.

18. Osias, J. R., "Finite Deformation of Elasto-Plastic Solids", NASA Contractor Report CR-2199, March 1973.

PLASTIC ANALYSIS OF MIXED MODE PLANE STRESS CRACK PROBLEMS*

J. W. Hutchinson and C. F. Shih
Harvard University, Cambridge, Massachusetts 02138

ABSTRACT

Two parameters are identified for characterizing the deformation in the plastic zone near the tip of a crack when mixed mode conditions prevail. Details of the near-tip stress and strain distributions are presented for hardening materials in which a diffuse plastic zone occurs under plane stress conditions. For small scale yielding the two near-tip parameters are related to the two elastic stress intensity factors for combined Mode I and Mode II.

PLASTIC STRESS AND STRAIN FIELDS FOR MIXED MODE CRACK PROBLEMS

Solutions to two dimensional crack problems in the plane for isotropic elasticity are characterized by the near-tip stress distribution

$$\sigma_{ij} = (2\pi r)^{-1/2}[K_I\sigma_{ij}^{I}(\theta) + K_{II}\sigma_{ij}^{II}(\theta)] , \qquad (1)$$

where r and θ are planar polar coordinates such that $\theta = 0$ directly ahead of the crack. The θ-variation of the Mode I contribution to the stresses is symmetric with respect to the crack tip while the Mode II contribution is antisymmetric. Mode I and II elastic stress intensity factors, K_I and K_{II}, constitute a two parameter characterization of the elastic near-tip field.

For two dimensional crack problems in which the material is modeled by a deformation theory of plasticity and in which the equilibrium equations and strain-displacement relations are taken to be linear, it can be shown that the strain energy density must vary like $1/r$ as the crack tip is approached [1, 2, 3]. Suppose a power hardening relation is assumed between the plastic strains and stresses so that in simple tension for "large" strains

$$\varepsilon^P \sim \alpha(\sigma/\sigma_o)^{n-1}\sigma/E . \qquad (2)$$

* This work was supported in part by the Air Force Office of Scientific Research under Grant AFOSR-73-2476, in part by the Advanced Research Projects Agency under Contract DAHC15-73-G-16, and by the Division of Engineering and Applied Physics, Harvard University.

Here σ_o is a reference stress which can be identified with the tensile yield stress if convenient, E is Young's modulus, n is the hardening exponent and α is a material constant. In this case the dominant singularity fields are of the form

$$\sigma_{ij} \sim r^{-1/(n+1)} \tilde{\sigma}_{ij}(\theta) \quad \text{and} \quad \varepsilon^P_{ij} \sim r^{-n/(n+1)} \tilde{\varepsilon}^P_{ij}(\theta) \ . \tag{3}$$

Details of these fields have been given for the pure modes in [1, 2, 3]. The θ-variations $\tilde{\sigma}_{ij}$ and $\tilde{\varepsilon}^P_{ij}$ depend implicitly on n and, in contrast to linearly elastic problems, depend in a significant way on whether plane stress or plane strain pertains.

The mixed mode crack tip fields for linear elasticity (1) are simply the superposition of the Mode I and Mode II contributions. The plasticity problem is inherently nonlinear so that a representation such as (1) cannot be used. As a measure of the relative amounts of Mode I and Mode II at the crack tip we introduce a near-tip mixity parameter M^P defined by

$$M^P = \frac{2}{\pi} \tan^{-1} \left| \lim_{r \to 0} \frac{\sigma_{\theta\theta}(r,\theta=0)}{\sigma_{r\theta}(r,\theta=0)} \right| \ . \tag{4}$$

With this choice M^P ranges from $M^P = 0$ for pure Mode II to $M^P = 1$ for pure Mode I.

The simplest deformation theory, J_2 deformation theory, has been used to generalize (2) to multiaxial states of stress. It is convenient to introduce the effective stress σ_e where $\sigma_e^2 = 3s_{ij}s_{ij}/2$ and $s_{ij} = \sigma_{ij} - \sigma_{pp}\delta_{ij}/3$. The near-tip fields can be represented in the form

$$\begin{aligned} [\sigma_{ij}, \sigma_e] &= \sigma_o K^P_M \, r^{-1/(n+1)} \, [\tilde{\sigma}_{ij}(\theta, M^P), \tilde{\sigma}_e(\theta, M^P)] \\ \varepsilon^P_{ij} &= (\alpha\sigma_o/E)(K^P_M)^n \, r^{-n/(n+1)} \, \tilde{\varepsilon}^P_{ij}(\theta, M^P) \ . \end{aligned} \tag{5}$$

The plastic stress intensity factor K^P_M can be thought of as the amplitude of the dominant singularity; the subscript M is attached to emphasize that, in general, it applies to mixed mode situations. This amplitude is given definite meaning by normalizing the maximum value of $\tilde{\sigma}_e$ to be unity where

$\tilde{\sigma}_e^2 = 3\tilde{s}_{ij}\tilde{s}_{ij}/2$ and $\tilde{s}_{ij} = \tilde{\sigma}_{ij} - \tilde{\sigma}_{pp}\delta_{ij}/3$. For a given value of n and for either plane stress or plane strain conditions, the functions $\tilde{\sigma}_{ij}$, $\tilde{\sigma}_e$ and $\tilde{\varepsilon}_{ij}^P$ are completely specified by the mixity parameter M^P . Details of these functions have been given for the case of plane strain in [4]; plane stress results will be discussed below.

Once the hardening exponent n is specified, K_M^P and M^P completely characterize the near-tip field. In place of the combination (K_M^P , M^P) it may be more convenient to introduce the path independent J integral [5] and to use the equivalent pair (J , M^P) . The three parameters are connected by [1]

$$J = (\alpha\sigma_o^2/E) I_n(M^P)(K_M^P)^{n+1} , \qquad (6)$$

where I_n is a numerical constant determined from the singularity analysis which depends on n and M^P . Plane strain values of I_n where given in [4] and plane stress values will be given below. In the pure mode cases M^P is known and thus J (or equivalently K_M^P) is a single parameter measuring the intensity of deformation in the near-tip field. But in the general mixed mode situation a pair of parameters is needed for a complete characterization.

PLANE STRESS NEAR-TIP FIELDS

Figure 1 gives the θ-variations of the stresses and strains in (5) for a relatively low strain hardening material with $n = 13$. Pure Mode I and pure Mode II are included along with two intermediate cases. The plane stress formulation used here is the same as employed in the Mode I study in [1]. It does not take into account the nonlinear geometric effect arising from sheet thinning. This, together with the assumption of a hardening material, leads to a diffuse plastic zone as opposed to the slender necking zone represented by the Dugdale model. Numerical methods used to calculate these quantities are discussed in [4] and in more detail in [6].

The angle θ^* at which the maximum amplitude of the tensile component $\sigma_{\theta\theta}$ is attained is plotted as a function of M^P for the entire range of n in Fig. 2a. (The curve for $n = \infty$ is from the perfect plasticity solution given in [6].)

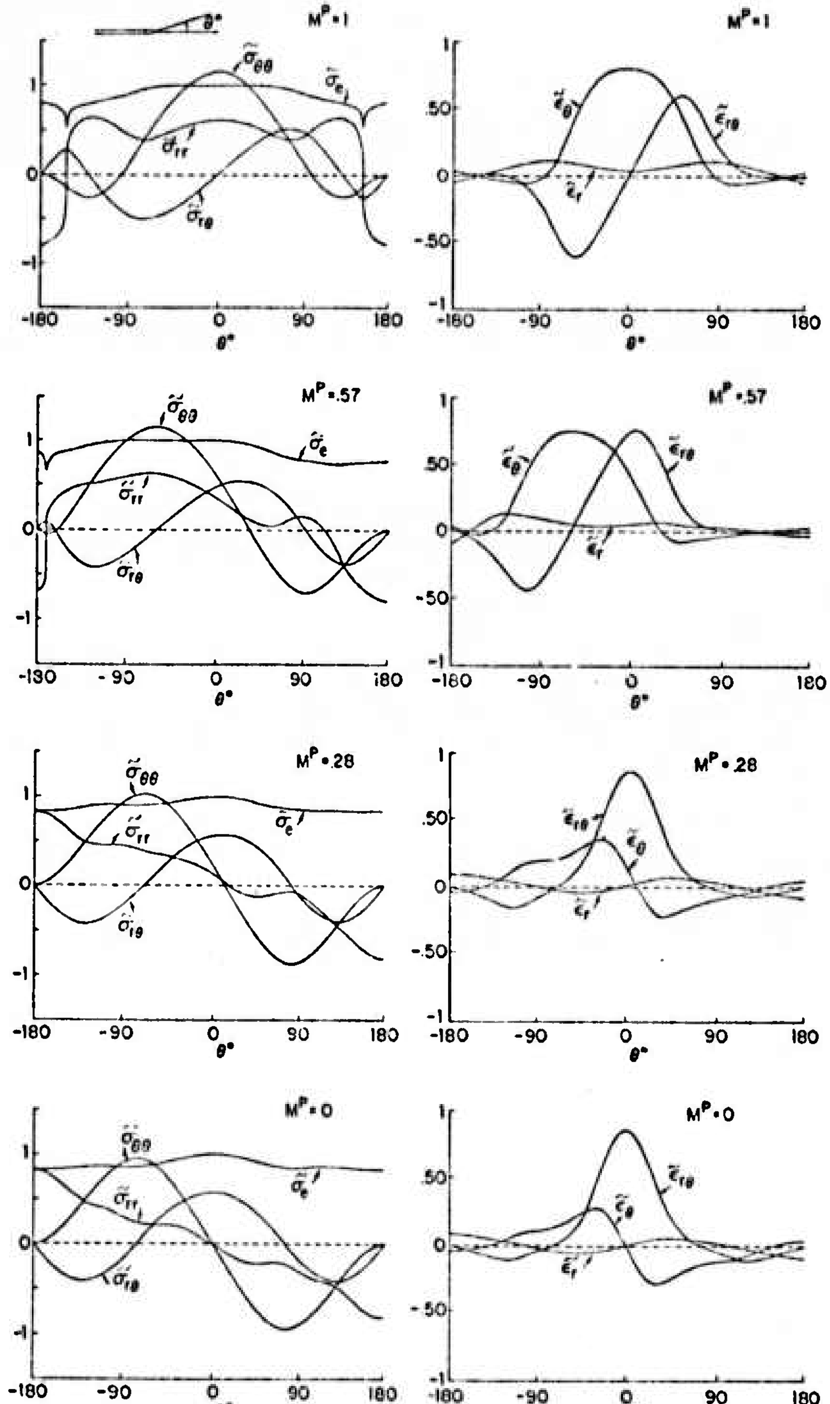

Fig. 1 θ-variations of stresses and strains at the tip of a crack for plane stress with $n = 13$.

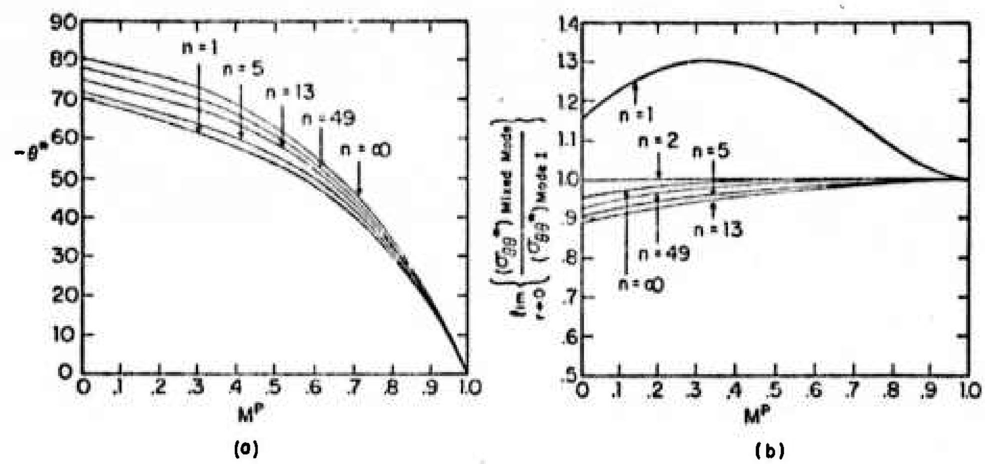

Fig. 2 (a) Angular position of maximum tensile stress θ^* (in degrees) as a function of the near-tip mixity parameter. (b) Ratio of the amplitude of the maximum tensile stress in mixed mode to that in Mode I for identical values of J .

The value of this maximum stress is normalized by the corresponding Mode I value, $\sigma_{\theta\theta}(\theta = 0)$, at the same r and same value of J . This ratio is shown as a function of M^P in Fig. 2b. Analogous curves for plane strain in [4] indicate a significant fall-off in the maximum tensile stress amplitude away from Mode I which is absent in plane stress.

Values of I_n , which enter into (6), are given in the form of curves in Fig. 3.

SMALL SCALE YIELDING

In the small scale yielding limit, when, roughly speaking, the plastic zone is small compared to the crack length and all other relevant geometric lengths, J can be expressed in terms of the elastic stress intensity factors according to (for plane stress [5])

$$J = (K_I^2 + K_{II}^2)/E . \qquad (7)$$

However it is not possible to obtain an analytic formula for M^P in terms of the elastic stress intensity factors. A full numerical analysis, such as that described in [4], must be employed to obtain this second relation. A convenient measure of the mixity for the <u>elastic</u> singularity solution (1) is given by the definition

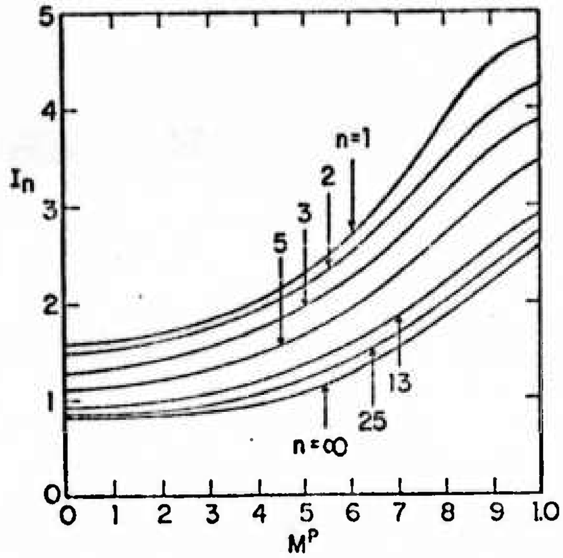

Fig. 3 Values of $I_n(M^P)$.

$$M^e = \frac{2}{\pi} \tan^{-1} \left| \lim_{r \to 0} \frac{\sigma_{\theta\theta}(r, \theta = 0)}{\sigma_{r\theta}(r, \theta = 0)} \right| = \frac{2}{\pi} \tan^{-1} \left| \frac{K_I}{K_{II}} \right| . \qquad (8)$$

(For a crack in an infinite sheet making an angle β (in radians) to a far pure tension field, $M^e = 2\beta/\pi$.) Either pair, (K_I , K_{II}) or (J , M^e) , completely specifies the near-tip field of the elastic mixed mode solution.

The results of the numerical analysis of the small scale yielding problem are shown in Fig. 4a in the form of plots of M^P as a function of M^e for various n . The curve labeled $n = \infty$ was obtained by extrapolation. The functional relation between M^P and M^e in plane stress small scale yielding is independent of Poisson's ratio and the amplitude of the singularity. It does depend implicitly on other shape details of the uniaxial stress-strain curve in addition to n . The results of Fig. 4 were obtained using the tensile relation $\varepsilon/\varepsilon_o = \sigma/\sigma_o$ for $\sigma \leq \sigma_o$ and $\varepsilon/\varepsilon_o = (\sigma/\sigma_o)^n$ for $\sigma > \sigma_o$, where $\varepsilon_o = \sigma_o/E$. As in [4], spot checks using other tensile curves give essentially the same results shown in Fig. 4 and it is concluded that n is the essential parameter. The corresponding relationship for plane strain from [4] is shown in Fig. 4b.

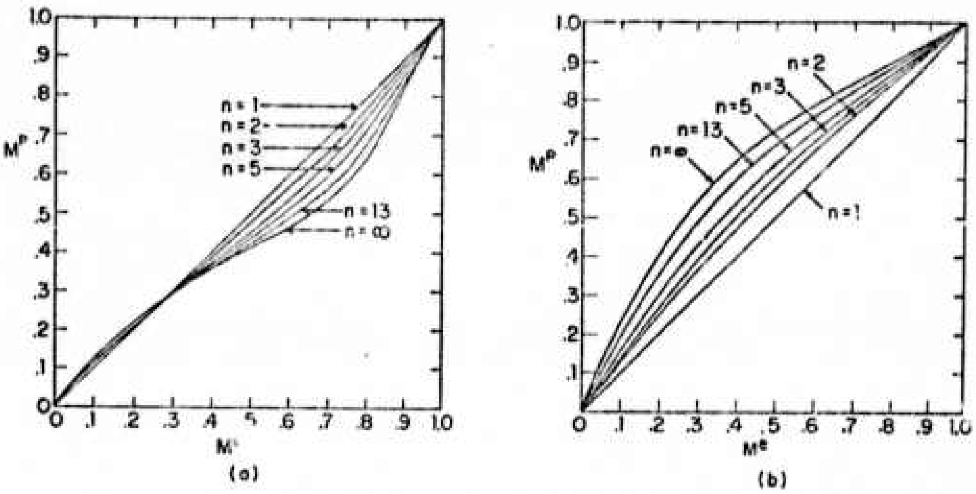

Fig. 4 Near-tip mixity M^P as a function of M^e for small scale yielding. (a) plane stress, (b) plane strain for $\nu = 0.3$ from [4].

The results of Fig. 2 may be reexpressed in terms of M^e using the connection between M^P and M^e. Thus, Fig. 5a shows the effect of the hardening exponent on the critical angle θ^* as a function of the elastic mixity parameter for small scale yielding in plane stress. The curves for plane strain from [4] are shown in Fig. 5b along with some experimental data on fracture initiation angles from [7, 8]. According to the plasticity analysis, a fairly wide range of fracture initiation angles about the elastic prediction $(n = 1)$ should be expected depending on the hardening exponent and on whether the plane stress or plane strain condition is approached.

Plastic zones for small scale yielding in plane stress are shown in Fig. 6 for four values of mixity. These zones were calculated using the power hardening law for uniaxial tension stated above. Mode I zones have been given earlier in [9] and are similar to those shown in Fig. 6 for $M^e = 1$, except that the present zones extend somewhat further ahead of the crack. It is felt that the present calculations are more accurate than those reported in [9].

REFERENCES

[1] J. W. Hutchinson, J. Mech. Phys. Solids 16, 13 (1968).
[2] J. W. Hutchinson, Ibid. 16, 337 (1968).
[3] J. R. Rice and G. F. Rosengren, Ibid. 16, 1 (1968).
[4] C. F. Shih, Small scale yielding analysis of mixed mode plane strain crack problems, Harvard University Report DEAP S-1, May 1973.

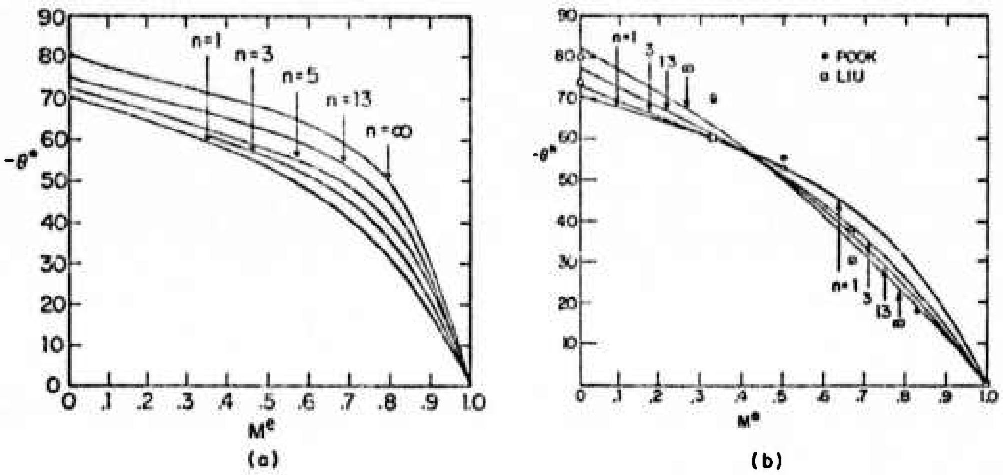

Fig. 5 θ^* (in degrees) as a function of M^e for small scale yielding. (a) plane stress, (b) plane strain.

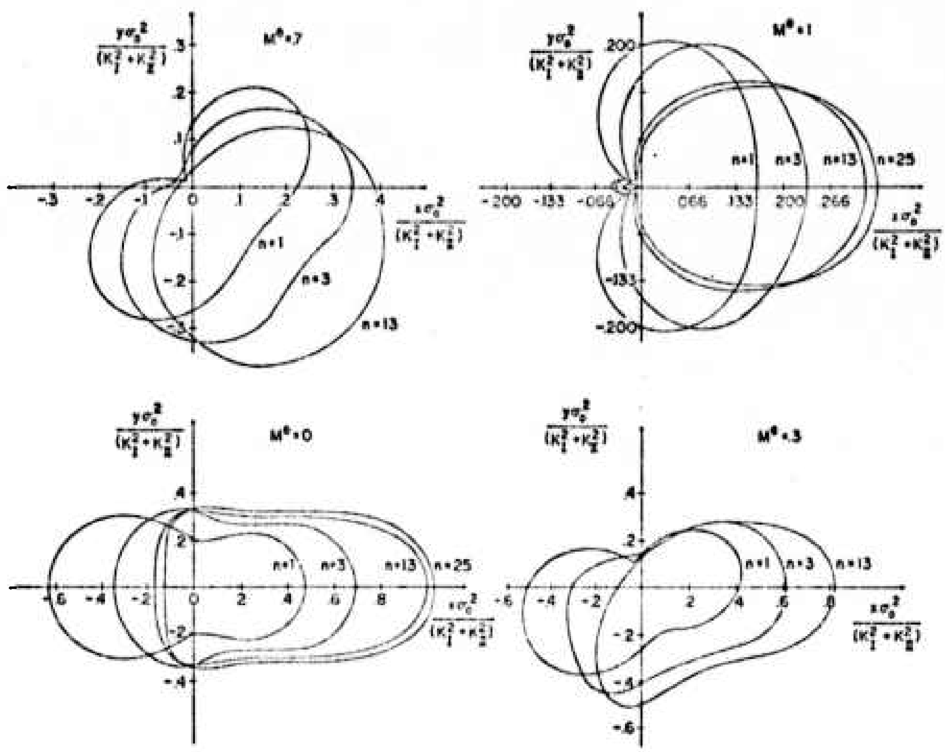

Fig. 6 Elastic-plastic boundaries for small scale yielding in plane stress.

[5] J. R. Rice, "Fracture" (edited by H. Liebowitz) (Academic Press, New York, 1968, 3, 191).
[6] C. F. Shih, Elastic-plastic analysis of combined mode crack problems, Ph.D. Thesis, Harvard University, 1973.
[7] A. F. Liu, AIAA Paper No. 73-253 (1973).
[8] L. P. Pook, Engng. Fract. Mech. 3, 205 (1971).
[9] P. D. Hilton and J. W. Hutchinson, Ibid. 3, 435 (1971).

Fully Plastic Crack in an Infinite Body Under Anti-plane Shear

by

John C. Amazigo
Department of Mathematics
Rensselaer Polytechnic Institute
Troy, New York 12181

ABSTRACT

The problem of a semi-infinite body with an edge crack subjected to far out-of-plane shear is solved by a transformation to a hodograph plane and the Wiener-Hopf technique. The material stress-strain behavior is governed by a pure power hardening relation and the results are valid for both deformation theory and flow theory of plasticity. Results are presented for crack opening displacement, path independent J integral, and crack tip singularities for all finite values of the power hardening parameter.

INTRODUCTION

The path independent J integral derived independently by Eshelby [1] and Rice [2,3] is generally recognized as a useful parameter that characterizes the near crack tip field due to stationary cracks in elastic media. More recent studies have demonstrated that this integral provides not only an accurate characterization of the crack tip elastic-plastic field but also a good elastic-plastic fracture criterion. Noteworthy among these studies are the analytic and experimental results of Begley and Landes [4,5] in which they propose Rice's J integral as a failure criterion. Bucci *et. al.* [6]

and Rice et. al. [7] have proposed estimation procedures for J. These procedures involve the use of plastically adjusted linear elastic results in conjunction with limit load analysis. Also proposed is the estimation of J from experimentally obtained single load vs. point load displacement results.

In this paper, we solve analytically the problem of a crack in an infinite body subjected to remotely applied anti-plane shear. The material stress-strain relation is governed by a power hardening law [8] - that is the normalized strain is equal to the normalized stress raised to some power. The results are therefore valid for fully plastic materials. Under the loading considered the stress history is proportional everywhere for monotonically increased loading and consequently the analysis is valid for both deformation theory and flow theory of plasticity. Results are presented for J and crack opening for the full range of the power hardening parameter that is from elastic to rigid-plastic materials. The problem for a finite strip under shear loading is under investigation, however, we note that the plane strain tensile loading of a strip has been solved by Goldman and Hutchinson [9] by the use of finite element method.

1. Fundamental Equations and the Hodograph Plane

We consider the semi-infinite body occupying the region $x \geq -a$, $-\infty < y, z < \infty$ (see Figure 1) with an edge crack of depth a represented geometrically by $-a < x < o$, $y = 0$. The body is subjected to remotely applied shearing stress τ_{∞}. By symmetry this problem is equivalent to the problem of the infinite body with a crack of width 2a subjected to the same remote loading. The only nonvanishing displacement component is the z component $w(x,y)$. Consequently, the nonvanishing strain components are $\gamma_{xz} = \partial w/\partial x$ and $\gamma_{yz} = \partial w/\partial y$. For small deformation and isotropic material, the corresponding stresses τ_{xz} and τ_{yz} are the only nonzero stress components. If we introduce the notation $\gamma_x = \gamma_{xz}$, $\gamma_y = \gamma_{yz}$, $\tau_x = \tau_{xz}$, and $\tau_y = \tau_{yz}$ then the compatibility and equilibrium equations reduce respectively to

$$\partial\gamma_x/\partial y = \partial\gamma_y/\partial x, \tag{1}$$

and

$$\partial\tau_x/\partial x + \partial\tau_y/\partial y = 0. \tag{2}$$

We consider a pure power hardening relation between the principal stress and strain given by

$$\gamma/\gamma_o = \alpha(\tau/\tau_o)^n, \tag{3}$$

where α is a nondimensional constant, γ_0 and τ_0 are reference principal strain and stress respectively, and n is the power hardening parameter. The principal stress and strain are

$$\tau = (\tau_x{}^2 + \tau_y{}^2)^{1/2}, \quad \gamma = (\gamma_x{}^2 + \gamma_y{}^2)^{1/2}. \tag{4}$$

It is clear that because of the relation (3) the governing equation for w is also nonlinear, however, the problem can be reduced to a linear problem by the hodograph transformation. In this transformation the roles of the dependent variables (γ_x, γ_y) and independent variables (x,y) are interchanged using implicit function theory. The transformation maps the physical plane in Figure 1 onto the strain or hodograph plane shown in Figure 2. The hodograph transformation was used by Rice [10] to obtain a perturbation solution for the same problem for elastic-plastic materials. Details of the subsequent derivation are contained in this reference. Neuber [11] used a stress hodograph plane to analyze the double-notched problem.

The application of this transformation to the compatability and equilibrium equations gives

$$\partial x/\partial \gamma_y = \partial y/\partial \gamma_x \tag{5}$$

and

$$\partial x/\partial \tau_x = \partial y/\partial \tau_y = 0 \tag{6}$$

Equation (5) implies the existence of a scalar potential function ψ such that

$$\vec{x} = \nabla_\gamma \psi \tag{7}$$

where $\vec{x}$ is the position vector and ∇_γ is the gradient operator with respect to the strain vector $\vec{\gamma} = (\gamma_x, \gamma_y)$. Further use of implicit function theory to relate differentiation with respect to τ_x, τ_y to differentiation with respect to γ_x, γ_y using (3) leads to the following linear partial differential equation

$$\frac{\partial^2 \psi}{\partial \gamma_x^{\,2}} + \frac{\partial^2 \psi}{\partial \gamma_y^{\,2}} + \frac{n-1}{\gamma}\left[\gamma_x^2 \frac{\partial^2 \psi}{\partial \gamma_x^{\,2}} + 2\gamma_x\gamma_y \frac{\partial^2 \psi}{\partial \gamma_x \partial \gamma_y} + \gamma_y^{\,2} \frac{\partial^2 \psi}{\partial \gamma_y^{\,2}}\right] = 0 \tag{8}$$

One boundary condition is that $x = -a$ on AB and DE in Figure 1 and this corresponds to

$$\partial \psi/\partial \gamma_x = -a \quad \text{for} \quad \gamma_x = 0,\ 0<\gamma_y<\gamma_\infty \tag{9}$$

where γ_∞ is the corresponding remotely applied strain. The other boundary condition is that $y = 0^+$, $-a<x<0$ on BC and DC and this leads to

$$\partial\psi/\partial\gamma_y = 0 \qquad \text{for} \qquad \gamma_y = 0. \tag{10}$$

It is convenient to introduce the nondimensional quantities

$$\rho = \gamma/\gamma_\infty, \; \Psi = \psi/a\gamma_\infty, \tag{11}$$

and a polar coordinate system (ρ,ϕ) such that

$$\gamma_x/\gamma_\infty = -\rho \sin\phi,$$

and (12)

$$\gamma_y/\gamma_\infty = \rho \cos\phi.$$

The differential equation (8) and boundary conditions (9) and (10) become

$$n\Psi,_{\rho\rho} + \frac{1}{\rho}\Psi,_{\rho} + \frac{1}{\rho^2}\Psi,_{\phi\phi} = 0, \; \rho>o, \; -\frac{\pi}{2}<\phi<\frac{\pi}{2} \tag{13}$$

$$\Psi,_{\phi} = 0, \qquad \phi = \pm\frac{\pi}{2}, \; \rho>0 \tag{14}$$

$$\Psi,_{\phi} = \rho, \qquad \phi = 0^{\pm}, \; 0<\rho<1 \tag{15}$$

where a comma subscript denotes partial derivative with respect to subsequent subscript(s).

2. Wiener-Hopf Problem

The problem consisting of equations (13)-(15) can be analyzed by a method which as noted in [12] was developed by Carleman but is generally referred to as the Wiener-Hopf technique. In order to apply integral transform we need the behavior of Ψ as $\rho\to o$ and $\rho\to\infty$.

By using equation (12) the relation (7) can be expressed in complex variable form as

$$-x/a + iy/a = \exp(-i\phi)(\psi,_\phi/\rho + i\psi,_\rho) \tag{16}$$

Now as $y \to o^+$, and $x \to -a$

$$\Psi,_\rho \to \sin\phi, \tag{17}$$

and

$$\Psi,_\phi \to \rho\cos\phi \quad \text{as } \rho \to o$$

thus, Ψ is bounded as $\rho \to o$.

For $\rho \to \infty$ we seek a solution to (13) and (14) of the form

$$\Psi \sim H(n,\phi)\rho^p.$$

Substituting for Ψ in equations (13) and (14) leads to

$$p = [1 - 1/n \pm \{(1-1/n)^2 + (2K + 1)^2/n\}^{1/2}]/2 \tag{18}$$

where K is an integer. Since Ψ must be bounded as $\rho \to \infty$, the maximum negative value of ρ must be chosen. This value is $p=-1/n$. Thus,

$$\Psi \to \rho^{-1/n} \quad \text{as} \quad \rho \to \infty. \tag{19}$$

We note that this leads to precisely the same singular behavior

$$\gamma \to (x^2 + y^2)^{-\frac{n}{2(n+1)}}$$

near the crack tip derived by Neuber [11] and Rice [10].

Now we introduce the Mellin transform $\overline{\Psi}$ of Ψ defined by

$$\overline{\Psi}(s,\phi) = \int_0^\infty \rho^{s-1}\Psi(\rho,\phi)d\rho. \tag{20}$$

By (13) this transform satisfies the equation

$$\overline{\psi},_{\phi\phi} + \omega^2(s)\,\overline{\psi} = 0, \quad 0<\text{Re } s<1/n \tag{21}$$

where

$$\omega^2(s) = s[n(s+1)-1], \tag{22}$$

and Re s denotes the real part of s. The strip $o<\text{Re } s<n$ of validity of the transform (21) follows from the behavior of Ψ as $\rho\to o, \infty$ given in the relations (17) and (19). The Mellin transform of (15) is

$$\overline{\Psi},_{\phi}(s,o) = \frac{1}{s+1} + \overline{u}(s), \quad \text{Re } s > -1 \tag{23}$$

where $\overline{u}$ is the transform of

$$u(\rho) = \begin{cases} o & o<\rho<1 \\ \psi,_{\phi}(\rho,o) & \rho>1 \end{cases} \tag{24}$$

For $\phi>o$ the solution of (21) and (23) is

$$\overline{\Psi}(s,\phi) = [\frac{1}{s+1} + \overline{u}(s)] \frac{\cos[\omega(s)(\phi-\pi/2)]}{\omega(s) \sin \pi/2\omega(s)}, \quad o<\text{Re } s<1/n \tag{25}$$

and for $\phi<o$,

$$\overline{\Psi}(s,-\phi) = - \overline{\Psi}(s,\phi).$$

Define

$$\overline{g}(s) = \overline{\Psi}(s,o^+) - \overline{\Psi}(s,o^-) \tag{26}$$

where $\Psi(s,o^+) = \lim_{\varepsilon\to o} \Psi(s,\varepsilon)$ for $\varepsilon>o$. Substituting this definition into equation (25) gives

$$\frac{1}{2}\, \overline{g}(s) = [\frac{1}{s+1} + \overline{u}(s)]P(s), \quad o<\text{Re } s<1/n \tag{27}$$

where

$$P(s) = \omega^{-1}(s) \csc \frac{\pi}{2}\, \omega(s) \cos [\omega(s)(\phi- \frac{\pi}{2})]. \tag{28}$$

We note that since Ψ must be continuous across the line $\phi= o$, $\rho>1$ the inverse transform $g(\rho)$ of $\overline{g}(s)$ must vanish for $\rho>1$ hence like $u(\rho)$, $g(\rho)$ is a half-known function. Furthermore, since $u(\rho)\to \rho^{-1/n}$ as $\rho\to\infty$ and $g(\rho)$ is bounded as $\rho\to o$ then $\overline{u}(s)$ is analytic for

Re s < 1/n and $\bar{g}(s)$ is analytic for Re s >o. Let us denote functions that are analytic in the left half plane Re s< 1/n by a subscript - and let a subscript + denote functions that are analytic for Re s > o. With this notation equation (27) becomes

$$\frac{1}{2}\,\bar{g}_+(s) = [(\frac{1}{s+1})_+ + \bar{u}_-(s)]p(s),\ o<\text{Re } s<1/n \qquad (29)$$

Equation (29) is now in the standard form for the application of the Wiener-Hopf technique (see for example [12], [13]).

3. Solution of the Wiener-Hopf Equation

The technique requires that p(s) be decomposed into the quotient

$$p(s) = N_-(n,s)/D_+(n,s) \qquad (30)$$

where $N_-(n,s)$ has no poles or zeros for Re s<1/n and $D_+(n,s)$ has no poles or zeros for Re s>o. It is noteworthy that although w(s) has branch points p(s) does not. The decomposition is readily accomplished by expressing the trigonometric functions in (28) in infinite product series.

Now, as given in [12],

$$\cos\frac{\pi}{2}\,\omega(s) = \prod_{k=1}^{\infty}\,[1-\frac{\omega^2(s)}{(2k-1)^2}].$$

Unless otherwise specified k ranges over all positive integers for all subsequent product series. An explicit separation of the terms leading to zeros in the respective half planes Re s>o and Re s<1/n gives

$$\cos\frac{\pi}{2}\,\omega(s) = \prod(\gamma^+_{2k-1}-a_{2k-1}s)\exp(a_{2k-1}\bar{s})\cdot\prod(a_{2k-1}s-\gamma^-_{2k-1})\exp(-a_{2k-1}\bar{s}), \qquad (31)$$

where

$$\bar{s} = s+(n-1)/2n \ , \ a_m = n^{1/2}/m, \tag{32}$$

and

$$\gamma_m^{\pm} = n^{1/2}\{1/n-1 \pm [(1-1/n)^2 + 4m^2/n]^{1/2}\}/2m.$$

The exponential products are introduced to render each series in (31) uniformly convergent [14]. Use has been made of the asymptotic behavior of γ_m as $m\to\infty$; namely,

$$\gamma_m^{\pm} = \pm\,[1 - \frac{n-1}{2\sqrt{n}}\cdot\frac{1}{m} + O(m^{-2})]. \tag{33}$$

Thus, the desired decomposition of p(s) is accomplished by setting

$$N_-(n,s) = B(n,s)\prod(\gamma_{2k-1}^{+}-a_{2k-1}s)\exp(a_{2k-1}\bar{s})/\prod(\gamma_{2k}^{+}-a_{2k}s)\exp(a_{2k}\bar{s}) \tag{34}$$

and

$$D_+(n,s) = \pi ns(s+1-1/n)B(n,s)\prod(a_{2k}s-\gamma_{2k}^{-})\exp(-a_{2k}\bar{s})/$$

$$2\prod(a_{2k-1}s-\gamma_{2k-1})\exp(-a_{2k-1}\bar{s})$$

where B(n,s) is an arbitrary function which will be chosen so that N_- and D_+ have algebraic behavior as $|s|\to\infty$ in the appropriate half-planes. The substitution of the quotient (30) for p(s) in (29) gives

$$\frac{1}{2}\,\bar{g}_+(s)\,D_+(n,s) = (\frac{1}{s+1})_+N_-(n,s) + \Pi_-(s)N_-(n,s), \quad 0<\mathrm{Re}\ s<1/n.$$

Now the first term on the right hand side of this equation can straightforwardly be decomposed into a sum. One such decomposition leads to

$$\frac{1}{2}\,\bar{g}_+(s)\;D_+(n,s) - N_-(n,-1)/(s+1) = [N_-(n,s) - N_-(n,-1)]/$$

$$(s+1) + \bar{u}_-(s)N_-(n,s), \qquad o<\text{Re } s<1/n. \tag{35}$$

Since the left hand side of equation (35) is analytic, in the right half plane Re $s>o$ and the right hand side is analytic in the left hand plane Re $s<1/n$ and these are equal on a strip $o<\text{Re } s<1/n$ each must be an analytic continuation of the other. Thus, each side represents the same entire function $E(s)$, say.

In order to determine $E(s)$ we need the asymptotic behavior of the functions $\bar{u}_-(s)$, $\bar{g}_+(s)$, $N_-(n,s)$, and $D_+(n,s)$ as $|s|\to\infty$.

Consider the asymptotic behavior of $N_-(n,s)$ as $|s|\to\infty$, Re $s<1/n$. We compare the behavior of $N_-(n,s)/B(n,s)$ as $|s|\to\infty$ with that of

$$M(s) = \prod(1-a_{2k-1}\bar{s})\exp(a_{2k-1}\bar{s})/\prod(1-a_{2k}\bar{s})\exp(-a_{2k}\bar{s}) \tag{36}$$

Now

$$\frac{N_-(n,s)}{B(n,s)M(s)} = \prod\frac{\gamma_{2k-1}-a_{2k-1}s}{1-a_{2k-1}\bar{s}}\;\prod\frac{\gamma_{2k}-a_{2k}s}{1-a_{2k}\bar{s}}$$

$$= \prod[1 + \beta_{2k-1}(s)]\;\prod[1 + \beta_{2k}(s)] \tag{37}$$

where $\beta_m = (\gamma_{2k-1}-1 + (n-1)a_{2k-1}/2n)/(1-a_{2k-1}\bar{s})$. Thus for Re $s<1/n$ and as a consequence of (33) $|\beta_m(s)| < (\text{constant})m^{-2}$. Hence each series in (37) converges uniformly and since $\lim\limits_{s\to\infty}\beta_m(s) = 0$ then

$$\lim_{s\to\infty}\frac{N_-(n,s)}{B(n,s)M(s)} = 1 \quad \text{for Re } s<1/n.$$

But M(s) is expressible in terms of gamma functions with well-known asymptotic behavior. Thus

$$N_-(n,s) \sim (-\pi s/2)^{1/2}\, n^{1/4}\, 2^{\bar{s}\sqrt{n}} B(n,s) \text{ as } |s|\to\infty,\ \text{Re } s<1/n$$

Consequently, the proper choice of B(n,s) is

$$B(n,s) = 2^{-s\sqrt{n}}\ , \tag{38}$$

and

$$N_-(n,s) \sim (-\pi s/2)^{1/2}\, n^{1/4}\, 2^{(n-1)/2\sqrt{n}} \quad \text{as } |s|\to\infty \tag{39}$$

Similarly,

$$D_+(n,s) \sim (\pi/2)^{1/2}\, n^{3/4}\, s^{3/2}\, 2^{(n-1)/2\sqrt{n}} \text{ as } |s|\to\infty, \text{Re } s>o \tag{40}$$

Now we consider the asymptotic behavior of $\bar{u}_-(s)$ and $\bar{g}_+(s)$. This behavior is dominated by the nature of $u(\rho)$ and $g(\rho)$ as $\rho\to 1^{\pm}$. This necessitates the study of Ψ in the neighborhood of $\rho=1$. Introduce the new variables ξ and η defined by

$$\xi = n^{1/2}\gamma_x/\gamma_\infty\ , \quad \eta = \gamma_y/\gamma_\infty - 1 \tag{41}$$

The partial differential equation (8) and boundary conditions (9) become

$$n\Psi,_{\xi\xi} + \Psi,_{\eta\eta} + \frac{n-1}{\frac{1}{n}\xi^2+(\eta+1)^2}[\xi^2\Psi_{\xi\xi} + 2\xi(\eta+1)\Psi_{\xi\eta} + (\eta+1)^2\Psi_{\eta\eta}]=0 \tag{42}$$

and

$$\Psi,_\xi(\xi=0^{\pm},\eta) = -\frac{1}{\sqrt{n}} \tag{43}$$

It is convenient to introduce polar coordinates (r_1,β) through the relations

$$\begin{aligned} \xi &= - r_1 \sin\beta \\ \eta &= r_1 \cos\beta \end{aligned} \tag{44}$$

For behavior of Ψ in the neighborhood of $\rho=1$ (i.e. $r_1=0$), an appropriate expansion of Ψ is

$$\Psi(r_1,\beta) = g_1(\beta)r_1^{1/2} + g_2(\beta)r_1 + 0(r_1^{3/2}) \tag{45}$$

whereupon substitution into (42) and equating power of r_1 the following differential equations are obtained for g_1, g_2:

$$g_1'' + \frac{1}{4}g_1 = 0 \tag{46}$$

$$g_2'' + g_2 = 0$$

where prime denotes differentiation with respect to the argument. The corresponding boundary conditions are

$$\begin{aligned} g_1'(\pm\pi) &= 0 \\ g_2'(\pm\pi) &= -n^{-1/2} \end{aligned} \tag{47}$$

The solutions to the boundary value problems are

$$g_1 = c_1 \sin(\alpha/2)$$

$$g_2 = n^{-1/2} \sin\alpha$$

where c_1 is an arbitrary constant. Thus as $r_1 \to 0$

$$\Psi \sim c_1 r^{1/2} \sin \alpha/2 + n^{-1/2} \sin\alpha \tag{48}$$

From this result and the relations (44), (41) and (12) it follows that

$$u(\rho) \sim (\text{constant})(\rho-1)^{-1/2} \quad \text{as} \quad \rho \to 1^+$$

and

$$g(\rho) \sim (\text{constant})(1-\rho)^{1/2} \quad \text{as} \quad \rho \to 1^-.$$

Hence by Watson's lemma [12]

$$\bar{u}_-(s) \to (-s)^{1/2} \quad \text{as } |s| \to \infty, \quad \text{Re } s < 1/n \tag{49}$$

and

$$\bar{g}_+(s) \to s^{-3/2} \quad \text{as } |s| \to \infty, \text{ Re } s > 0. \tag{50}$$

Now from the asymptotic relations (49), (50), (39), and (40) we conclude that the entire function E(s) is bounded as $|s|\to\infty$, and hence by Liouville's theorem it must be a constant K(n), say. Thus, from (35)

$$\frac{1}{s+1} + \bar{u}_-(s) = \frac{F(n,s)}{(s+1)N_-(n,s)} \tag{51}$$

where

$$F(n,s) = N_-(n,-1) + (s+1)K(n) \tag{52}$$

Substituting the result (51) in equation (25) and invoking the inversion formula for the Mellin transform gives

$$\Psi(\rho,\phi) = \frac{1}{2\pi i}\int_{c-i\infty}^{c+i\infty} \rho^{-s}\,\frac{F(n,s)\cos[\omega(s)(\phi-\pi/2)]}{(s+1)N_-(n,s)\,\omega(s)\sin\frac{\pi}{2}\omega(s)}\,ds \quad o<c<1/n \tag{53}$$

We now apply the theory of residues to the evaluations of this integral. The integrand has simple poles for $n\neq 1,\infty$ at $s=o$, $-1+1/n$, -1, $2m\gamma_{2m}^{-}n^{-1/2}$ and $(2m-1)\gamma_{2m-1}^{+}n^{-1/2}$, $m=1,2,\ldots$. By Jordan's lemma, for $\rho>1$ we close the contour by a large semicircle in the half plane Re $s>o$ along which the integrand is small. Similarly, for $\rho<1$ the contour is appropriately closed in the half plane Re $s<o$. It follows from residue theorem that

$$\Psi(\rho,\phi) = \begin{cases} \dfrac{2F(n,o)}{\pi(n-1)N_-(n,o)} + \dfrac{2nF(n,-1+1/n)}{\pi(n-1)N_-(n,-1+1/n)}\rho^{1-1/n} + \rho\sin\phi \\[2ex] + \dfrac{1}{\pi}\displaystyle\sum_{m=1}^{\infty} \dfrac{F(n,b_m)}{m(1+b_m)N_-(n,b_m)\omega'(b_m)}\rho^{-b_m}\cos 2m\phi, \quad o<\rho<1 \\[2ex] \displaystyle\sum_{m=1}^{\infty} \dfrac{2\sqrt{n}C_m F(n,C_m)\prod_{k=1}^{\infty}(\gamma^+_{2k}-a_{2k}C_m)\exp(a_{2k}\bar{C}_m)}{n^{1/2}(1+C_m)\prod_{\substack{k=1\\k\neq m}}^{\infty}(\gamma^+_{2k-1}-a_{2k-1}C_m)\exp(a_{2k-1}\bar{C}_m)}\rho^{-C_m}\sin(2k+1)\phi, \quad \rho>1 \end{cases} \tag{54}$$

where

$$C_m = (2m-1)\gamma^+_{2m-1}n^{-1/2}, \quad \bar{C}_m = C_m + (n-1)/2n, \text{ and}$$

$$b_m = 2m\gamma^-_m n^{-1/2}, \text{ and } \gamma^{\pm}_m \text{ are given by equation (32).}$$

There remains only the unknown $K(n)$ contained in the expression for $F(n,s)$. This constant is determined by imposing the condition (17). For Ψ_ρ to be bounded as $\rho\to o$ $F(n,-1+1/n)$ must vanish; hence

$$K(n) = -nN_-(n,-1) \tag{55}$$

and consequently,

$$F(n,s) = N_-(n,-1)[1-n(s+1)] \tag{56}$$

The combination of equations (54) and (16) provides a complete solution to the problem.

4. J Integral and Crack Opening Displacement

We compute here the path independent J integral [2] given by

$$J = \int_{\Gamma} [W dy - \vec{T} \cdot \frac{\partial \vec{u}}{\partial x} ds] \qquad (57)$$

where Γ is any simple contour in the xy-plane, W is the strain energy density, $\vec{T}$ is the stress vector acting on the outer side of Γ and $\vec{u}$ is the displacement vector. For the mode of loading considered here (57) can be reduced to

$$J = - \frac{a\, \tau_o\, \gamma_\infty^{1+1/n}}{(\alpha \gamma_o)^{1/n}}\, n\, \rho^{2+1/n} \frac{\partial^2}{\partial \rho^2} \int_{-\pi/2}^{\pi/2} \Psi \sin\phi d\phi. \qquad (58)$$

Now from (54)

$$\Psi \to Q(n) \rho^{-1/n} \sin \phi \quad \text{as } \rho \to \infty \qquad (59)$$

where

$$Q(n) = - \frac{n^{3/2} 2^{\sqrt{n}} N_-(n,-1)}{n+1} \frac{\prod (\gamma^+_{2k} - \frac{1}{2k\sqrt{n}}) \exp(n+1)/4k\sqrt{n})}{\prod (\gamma_{2k+1} - \frac{1}{(2k+1)\sqrt{n}}) \exp((n+1)/2(2k+1)\sqrt{n})} \qquad (60)$$

Although the asymptotic result (59) is valid for all $n \neq \infty$, its region of validity decreases as n increases since other terms in (54) become increasingly significant in comparison to (59).

Substitution of (59) into equation (58) and performing the elementary manipulation gives

$$J = - a\tau_\infty \gamma_\infty Q(n)(n+1)/2n \qquad (61)$$

The elimination of τ_∞ using (3) gives the equivalent result

$$J = -a\tau_o \gamma_o \alpha^{-1/n} (\gamma_\infty/\gamma_o)^{(n+1)/n} Q(n)(n+1)/2n \qquad (62)$$

J is computed by evaluating the infinite product series using double precision arithmetic. The results which are accurate to five significant figures are exhibited in Table I and presented graphically in Figure 3. Although we were unable to prove the following behavior of J,

$$J \approx (\pi/2)^{3/2}\, n^{1/2} \text{ as } n\to\infty \tag{63}$$

nevertheless because of the importance of such a formula we present it here and compare it graphically with the exact value in Figure 3.

Table 1

n	$\dfrac{J}{\tau_0\gamma_0 a\alpha^{-1/n}\left(\frac{\gamma_\infty}{\gamma_0}\right)^{\frac{n+1}{n}}}$	$\dfrac{S}{a\gamma_0\left(\frac{\gamma_\infty}{\gamma_0}\right)}$
1.0	1.5708	2.0000
1.5	1.9389	2.3338
2.0	2.2709	2.6444
3.0	2.8638	3.2090
5.0	3.8654	4.1748
10.0	5.7878	6.0445
20.0	8.5240	8.7267
30.0	13.865	14.008
50.0	19.802	19.915
100.0	63.182	63.370

The crack opening displacement δ is defined by

$$\delta = w(x=-a,y=o^+) - w(x=-a,y=o^-). \tag{64}$$

From $\gamma_x = \partial w/\partial x$, $\gamma_y=\partial w/\partial_y$ and the relation (7) it follows that

$$w = \vec{\gamma}\cdot\nabla_\gamma\psi - \psi + \text{const} \tag{65}$$

which is a Legendre transformation. Substituting for ψ in (65) using (54) and (11) leads to

$$\frac{\delta}{a\gamma_o(\frac{\gamma_\infty}{\gamma_o})} = \frac{4N_-(n,-1)}{\pi N_-(n,o)} \tag{66}$$

This expression was evaluated numerically and the results are given in Table 1 and displayed in figure 4. As for the J integral the behavior of δ as $n \to \infty$ is represented by the unproven formula

$$\delta \approx (\pi/2)^{3/2} n^{1/2} \tag{67}$$

In figure 5 the dependence of $J/[\tau_o \gamma_o a(\delta/a\gamma_o)^{\frac{n+1}{n}}]$ on n is given. Thus, a knowledge of the power hardening parameter n and the crack opening displacement is sufficient for the determination of J integral. Such a relation may prove very useful in light of the recent experimental and analytic estimation procedures [4,6,7] for J.

The stress, strain, and displacement fields in the neighborhood of the crack can be calculated in terms of J using the asymptotic result (59). Let (r,θ) be polar coordinates centered at the crack tip in the physical xy-plane (see Figure 1) then

$$\begin{Bmatrix} \gamma_{xz} \\ \gamma_{yz} \end{Bmatrix} = \gamma_\infty \kappa \left(\frac{ah(\theta)}{r}\right)^{\frac{n}{n+1}} \begin{Bmatrix} -\sin\phi \\ \cos\phi \end{Bmatrix} \tag{68}$$

and

$$w = a\kappa\left(\frac{ah(\theta)}{r}\right)^{\frac{-1}{n+1}} \sin\phi$$

where

$$\kappa = \left(\frac{J}{\tau_o \gamma_o a \alpha^{-1/n} \left(\frac{\gamma_\infty}{\gamma_o}\right)^{n+1}} \cdot \frac{2}{\pi}\right)^{\frac{n}{n+1}},$$

$$2\phi = \theta + \arcsin\left(\frac{n-1}{n+1}\sin\theta\right), \quad h(\theta) = \frac{\sin 2\phi}{2\sin\theta}.$$

The expression for the stress is omitted since it is readily obtained by using (3). The nature of the behavior in (66) was noted by Hilton and Hutchinson [15]. Here, however, the near crack tip fields are expressed in terms of Rice's J integral. For n=1 the results (62), (65), and (67) reduce to the well-known results for elastic material; namely,

$$J = \pi\tau_0\gamma_0 a\alpha^{-1}(\gamma_\infty/\gamma_0)^2/2, \quad \delta = 2a\gamma_0(\gamma_\infty/\gamma_0),$$

and

$$\begin{pmatrix}\tau_{xz}\\ \tau_{yz}\end{pmatrix} = \frac{K_{111}}{(2\pi r)^{1/2}}\begin{pmatrix}-\sin\theta/2\\ \cos\theta/2\end{pmatrix} \quad \text{with } K_{111} = \tau_\infty(\pi a)^{1/2}.$$

Acknowledgement

This work was supported in part by the Air Force Office of Scientific Research under Grant AFOSR-73-2476, in part by the Advanced Research Projects Agency under Contract DAHC 15-73-G-16 and by the Division of Engineering and Applied Physics, Harvard University, and in part by the National Science Foundation under Grant GP33679X with Rensselaer Polytechnic Institute. The author acknowledges with pleasure several helpful discussions with J. R. Rice, E. W. Hart, and J. W. Hutchinson who suggested the problem. The analysis presented here was begun while the author was a Research Fellow at Harvard during the summer of 1973.

References

1. J.D. Eshelby, "The Energy Momentum Tensor in Continuum Mechanics", Inelastic Behavior of Solids, ed. M.F. Kanninen et.al., McGraw Hill, 1970.

2. J.R. Rice, "A Path Independent Integral and the Approximate Analysis of Strain Concentrations by Notches and Cracks", J. Applied Mechanics, Vol. 35, pp. 379-386 (1968).

3. J.R. Rice, "Mathematical Analysis in the Mechanics of Fracture", Fracture, An Advanced Treatise, Vol. II, ed. H. Liebowitz, Academic Press, 1968, pp. 191-311.

4. J.A. Begley and J.D. Landes, "The J Integral as a Fracture Criterion", Fracture Toughness, ASTM, STP 514, American Society for Testing and Materials, pp. 1-20, (1972).

5. J.D. Landes and J.A. Begley, "The Effect of Specimen Geometry on J_{Ic}", Ibid., pp. 24-39 (1972).

6. R.J. Bucci, P.C. Paris, J.D. Landes and J.R. Rice, "J Integral Estimation Procedure", Ibid., pp. 40-69 (1972).

7. J.R. Rice, P.C. Paris and J.G. Merkle, "Some Further Results of J Integral Analysis and Estimates", Ibid., pp. 231-245 (1973).

8. A.A. Ilyushin, "The Theory of Small Elastic-Plastic Deformations", Prikladnaia Matematika i Mekhanika, Vol. 10, pp. 347-356 (1946).

9. N.L. Goldman and J.W. Hutchinson, "Fully Plastic Crack Problems: The Center-Cracked Strip in Plane Strain", DEAP Report 5-6, Harvard University (1974).

10. J.R. Rice, "Stresses Due to a Sharp Notch in a Work-Hardening Elastic-Plastic Material Loaded by Longitudinal Shear", J. Applied Mechanics, Vol. 34, pp. 287-298 (1967).

11. H. Neuber, "Theory of Stress Concentration for Shear-Strain Prismatical Bodies with Arbitrary Non-Linear Stress Strain Law", J. Applied Mechanics, Vol. 28, pp. 544-550 (1961).

12. G.F. Carrier, M. Krook, and C.E. Pearson, Functions of a Complex Variable: Theory and Technique, McGraw-Hill, 1966.

13. B. Noble, Methods Based on the Wiener-Hopf Technique for the Solution of Partial Differential Equations, Pergamon Press, 1958.

14. A.I. Markushevich, Theory of Functions of a Complex Variable, Vol. II, Translated from the Russian by A. Silverman, Prentice Hall, 1965.

15. P.D. Hilton and J.W. Hutchinson, "Plastic Intensity Factors for Cracked Plates", Engineering Fracture Mechanics, Vol. 3, pp. 435-451 (1971).

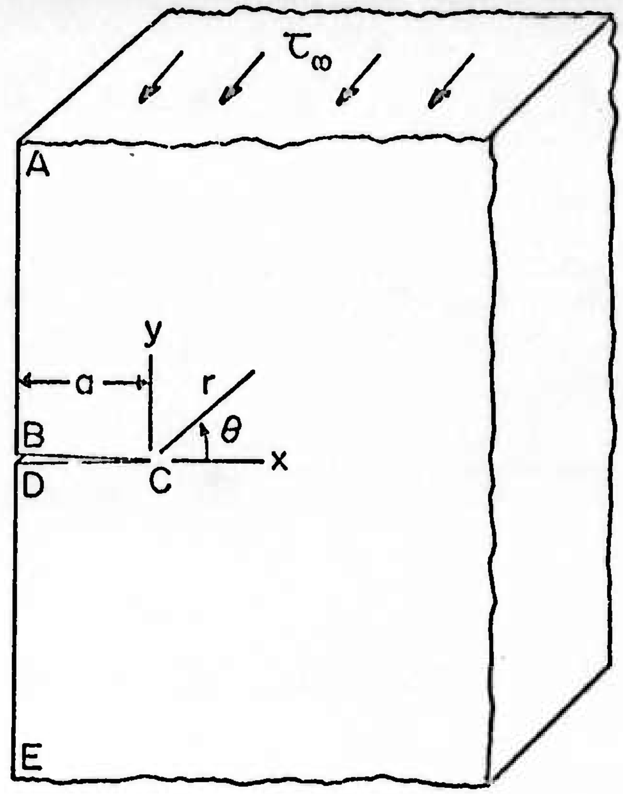

FIG. 1 GEOMETRY

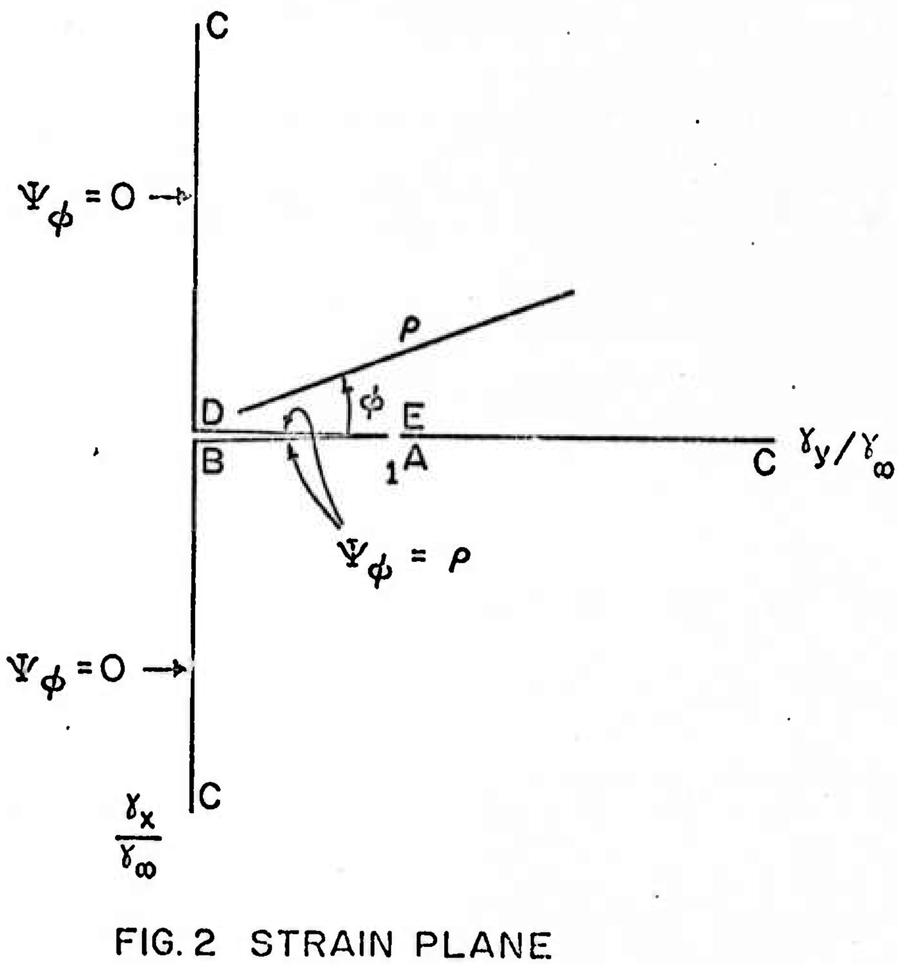

FIG. 2 STRAIN PLANE

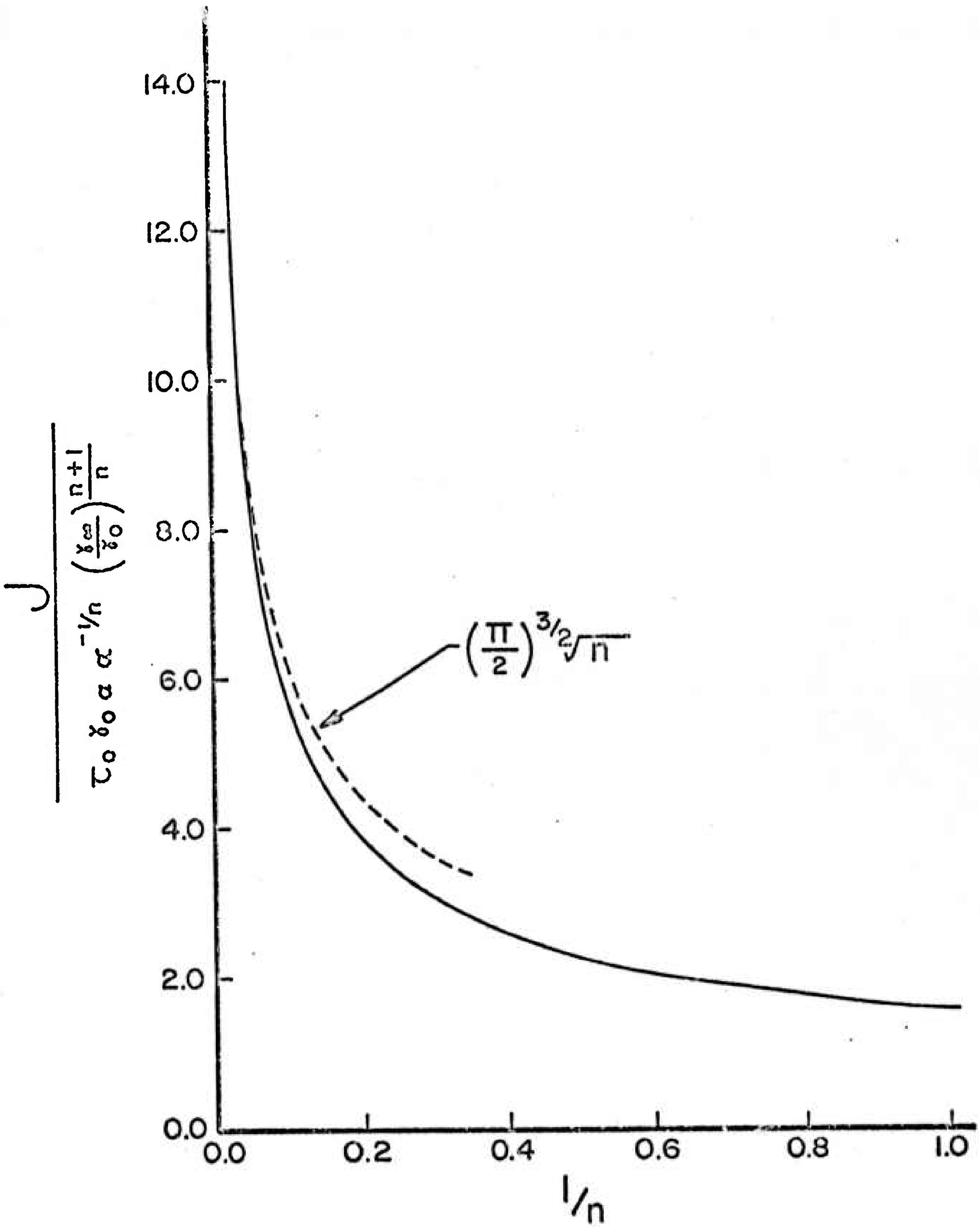

FIG. 3 J-INTEGRAL

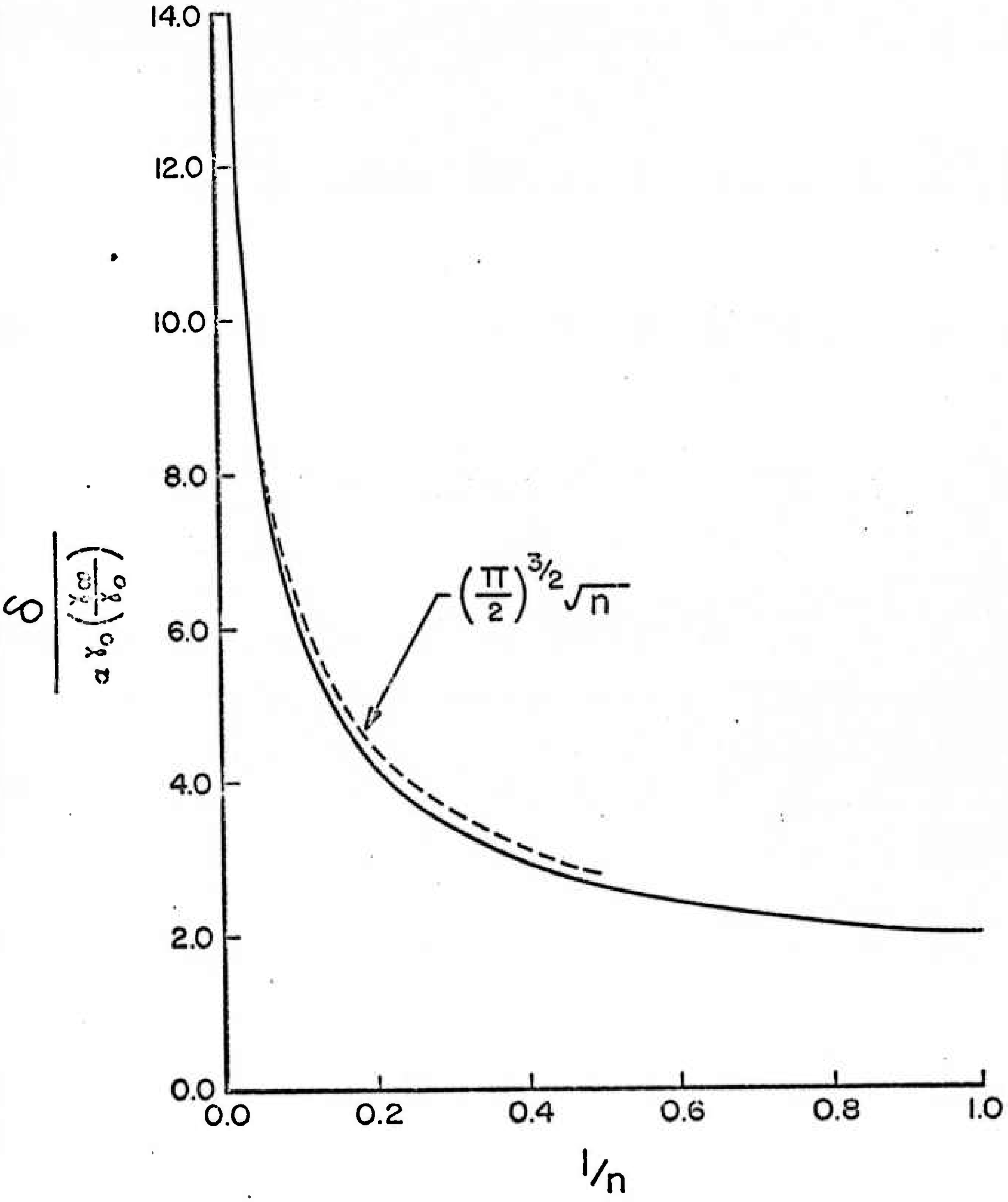

FIG. 4 CRACK OPENING DISPLACEMENT

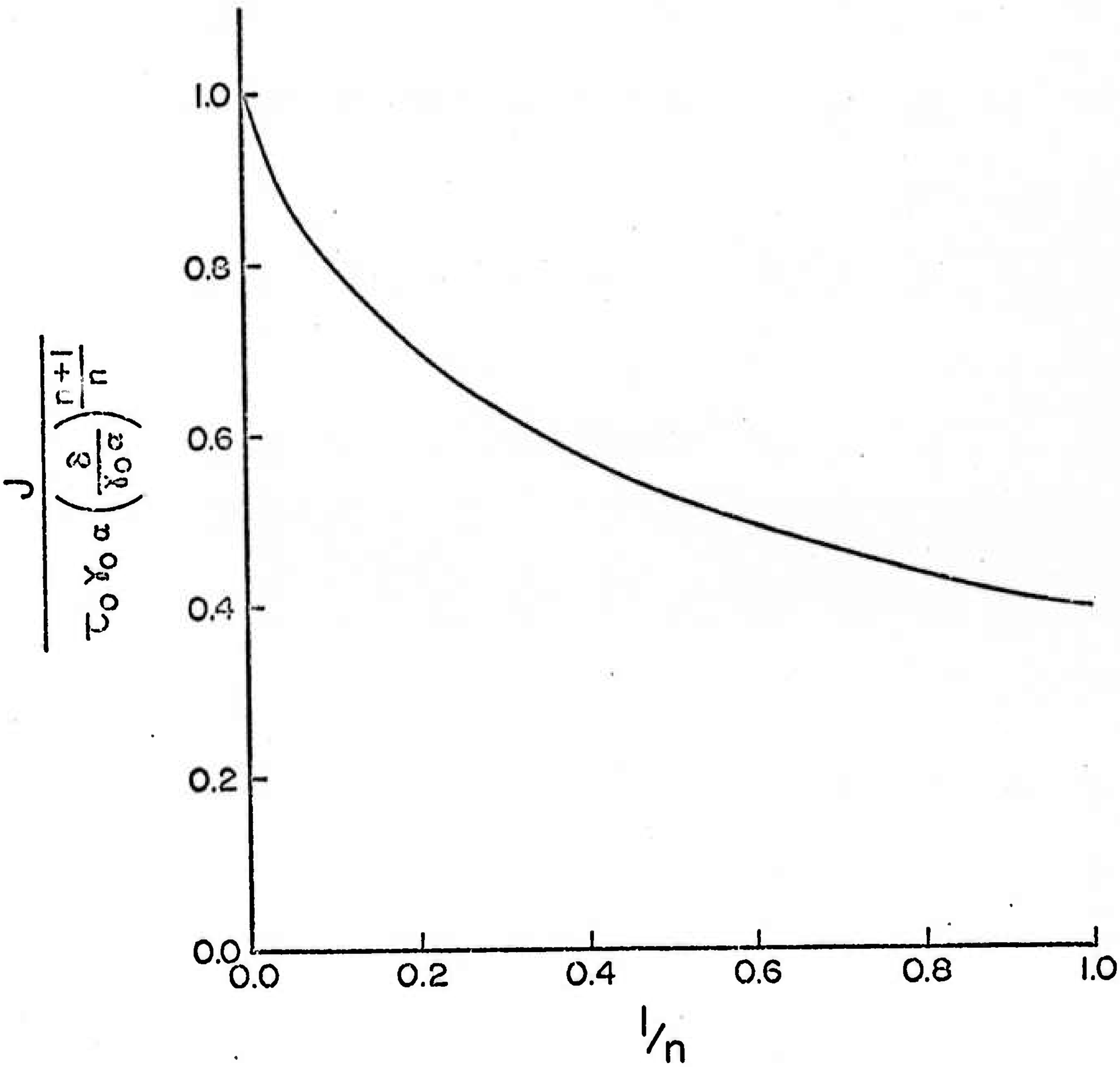

FIG. 5 J-δ RELATION

III. SUPERCONDUCTIVITY RESEARCH--LAYERED MATERIALS

Profs. M. Tinkham, M. R. Beasley

Report Summary

Research at Harvard into the properties of superconducting layered compounds is aimed at understanding the nature of the superconductivity in this important new class of materials. In order to establish the nature and strength of the superconducting coupling between individual metallic layers and to understand the high field superconductivity of these materials, we have measured the superconducting upper critical fields of certain layered compounds. These compounds can also have organic molecules intercalated between layers. A sensitive, orientable AC-susceptibility apparatus has been designed and built to make these measurements in low fields; a high field instrument is presently under construction. Our results for intercalated TaS_2 for a series of organic molecules, confirm for the first time that the anisotropy of magnetic properties increases markedly with increasing layer spacing.

Superconducting layered compounds, such as $NbSe_2$ and TaS_2, comprise a newly discovered class of superconductors, in which the spacing between the individual metallic layers can be increased from 3 Å up to 50 Å by intercalation of organic molecules (e.g. $TaS_2(\text{pyridine})_{1/2}$). Although much progress has been made in determining how the superconducting transition temperatures of these compounds depend on layer material, alloy composition, and especially layer spacing, comparatively little is known about the more general superconducting properties, such as the upper critical magnetic field, H_{c2}. The H_{c2} values represent the maximum field up to which superconductivity persists, and in these materials can be extremely high, and hence of considerable interest. Measurements of H_{c2} provide significant information on the effect of layer separation on interlayer coupling, as well as information on intrinsic material parameters of the metallic layers.

We are currently measuring the upper critical fields of TaS_2 intercalated with a series of different organic molecules with various layer spacings, and TaS_xSe_{1-x} and its intercalated compounds. These materials can have extremely high H_{c2} values ($\sim$200 kGauss at $T = 0$) with strong anisotropy for different field orientations. To study these critical fields, we have developed a sensitive, orientable instrument to measure H_{c2} by means of an AC susceptibility measurement. To date we have completed measurements in low fields (to 15 kGauss) for three intercalates of TaS_2. In addition, an instrument capable of expanding these measurements to high fields (130 kGauss) has been designed for a high-field magnet here at Harvard, and is presently being constructed. It is expected that deviations at high fields from extrapolations based on our measurements at low fields will provide additional important information about these materials. The high-field behavior has been investigated theoretically in a collaborative effort between R. Klemm and Professors Beasley and Luther.[1]

Results to date for low fields include those for $TaS_2(\text{collidine})_{1/6}$ [3 Å additional space between layers due to the collidine], $TaS_2(\text{pyridine})_{1/2}$ [6 Å], and $TaS_2(\text{aniline})_{3/4}$ [12 Å]. We find that as the space between layers increases from 3 Å to 12 Å, the superconducting coupling between metal layers becomes weaker, and the anisotropy increases markedly. These initial results for this series of compounds are confirmation of the expectation that very high-field superconductivity, of highly anisotropic two-dimensional character will result for the largest layer spacing between layers. Such conclusions could not be drawn from an investigation which did not study a specific <u>series</u> of compounds, even if many varied materials were studied.

We intend in the immediate future to extend these measurements to high fields and to numerous other superconducting layered compounds and organic intercalates. Hopefully, such a systematic study will enable us to establish a coherent picture of the superconducting magnetic properties of these compounds.

Reference:

1. R. A. Klemm, M. R. Beasley, and A. Luther, to be published.

Superconductors with Strong Flux-Pinning Characteristics

The objective of this research project is the production of a class of superconducting materials capable of carrying large currents without dissipation in the presence of high magnetic fields. Such superconductors must have a high density of pinning sites which prevent the movement of magnetic flux through the material. Voids are among the best pinning sites known. To be effective, they must be small enough to be present in great numbers but large enough to constitute significant energy barriers for flux lines. The minimum diameter of an effective flux-pinning void is approximately the superconducting coherence length which is typically 50 to 100 Angstroms (about 10^{-8} meter) for high-field superconductors.

The question we faced was how to produce a bulk superconductor containing a high density of such tiny holes. Our solution was to form the material by compacting a very finely divided powder to less than 100% density. This powder had to be a superconductor prior to compacting or had to be convertible to a superconductor during the subsequent sintering of the compact.

To date we have completed the development of a process utilizing spray-drying to make a finely divided amorphous powder containing niobium, chlorine, oxygen, carbon, and hydrogen. We heat this intermediate product to 700°C. in ammonia to form niobium nitride or to 850°C. in methane and hydrogen to form niobium carbide. Finely divided niobium pentoxide, dioxide, and monoxide can also be made at selected temperatures by using hydrogen alone as the reducing agent. By modifying the starting materials and the chemical treatment which follows spray-drying, a variety of finely divided compounds, elements, and alloys of interest to the physicist and metallurgist can be produced. At the moment we are principally interested in niobium nitride.

We have learned to control the many parameters of the process so that batches of crystallites with mean sizes as small as 150 Angstroms can be made, and we have developed compacting techniques which can form these powders into long, thin rods with smooth surfaces. We have also sintered these rods into strong superconducting materials which have crystal structures favorable to high transition temperatures and which show evidence of good internal contact in spite of their desirable degree of porosity.

To prepare these samples, we have constructed a furnace system with a large adjoining glove box in which the processes necessary to convert the spray-dried powder into a sintered pellet can be carried out in an inert atmosphere to protect the finely divided materials from contamination. We have also built the low temperature equipment necessary to measure the superconducting transition temperatures and the magnetization curves from which flux-pinning characteristics can be inferred.

Our next task will be to adjust the metallurgical and chemical properties of the rods to optimize their superconducting properties. Specific attention will be given to the maximization of the superconducting transition temperature by the control of stoichiometry and to the maximization of the current carrying capacity by the control of mean density.

It is our hope that these experiments will enable an evaluation of the efficacy of void-impregnated bulk materials as high-field, high-current superconductors.